

Key Points:

- Ensemble-based simulations of future shoreline evolution to 2100, including sea-level rise driven erosion, are performed and analyzed
- Future shoreline projections uncertainties are initially controlled by modeling assumptions and after 2060 by sea-level rise uncertainties
- The choice of wave-driven equilibrium modeling approach and incident wave chronology are critical to short/mid-term shoreline projections

Supporting Information:

Supporting Information may be found in the online version of this article.

Correspondence to:

M. D'Anna,
m.danna@brgm.fr

Citation:

D'Anna, M., Castelle, B., Idier, D., Rohmer, J., Le Cozannet, G., Thieblemont, R., & Bricheno, L. (2021). Uncertainties in shoreline projections to 2100 at Truc Vert beach (France): Role of sea-level rise and equilibrium model assumptions. *Journal of Geophysical Research: Earth Surface*, 126, e2021JF006160. <https://doi.org/10.1029/2021JF006160>

Received 11 MAR 2021

Accepted 28 JUN 2021

Uncertainties in Shoreline Projections to 2100 at Truc Vert Beach (France): Role of Sea-Level Rise and Equilibrium Model Assumptions

M. D'Anna^{1,2} , B. Castelle² , D. Idier¹ , J. Rohmer¹, G. Le Cozannet¹ , R. Thieblemont¹, and L. Bricheno³ 

¹BRGM, French Geological Survey, Orléans, France, ²Université de Bordeaux, UMR EPOC, CNRS, Pessac, France, ³National Oceanography Center, Liverpool, UK

Abstract Sandy shorelines morphodynamics responds to a myriad of processes interacting at different spatial and temporal scales, making shoreline predictions challenging. Shoreline modeling inherits uncertainties from the primary driver boundary conditions (e.g., sea-level rise and wave forcing) as well as uncertainties related to model assumptions and/or misspecifications of the physics. This study presents an analysis of the uncertainties associated with future shoreline evolution at the cross-shore transport dominated sandy beach of Truc Vert (France) over the 21st century. We explicitly resolve wave-driven shoreline change using two different equilibrium modeling approaches to provide new insight into the contributions of sea-level rise, and free model parameters uncertainties on future shoreline change in the frame of climate change. Based on a Global Sensitivity Analysis, shoreline response during the first half of the century is found to be mainly sensitive to the equilibrium model parameters, with the influence of sea-level rise emerging in the second half of the century (~2050 or later), under several simulated scenarios. The results reveal that the seasonal and interannual variability of the predicted shoreline position is sensitive to the choice of the wave-driven equilibrium-based model. Finally, we discuss the importance of the chronology of wave events in future shoreline change, calling for more continuous wave projection time series to further address uncertainties in future wave conditions. Our contribution demonstrates that unmitigated climate change can result in shoreline retreat of several tens of meters by 2100, even for sectors that have been stable or slightly accreting over the last century.

1. Introduction

Ongoing climate change is one of the largest concerns of our time, and its largest impacts on the world's environment are yet to come. Global mean sea-level rise is accelerating since 1870, and is expected to continue rising over the 21st century, although acceleration may be avoided if the Paris Agreement “below 2°C climate warming” target is met (Church et al., 2013; Oppenheimer et al., 2019). In addition, global wave power is adapting to the sea surface temperature since the late 1940s (Reguero et al., 2019), and is expected to change along with storminess by 2100 (Morim et al., 2020).

Sandy beaches provide precious natural, structural and social-economical resources to coastal communities (Ghermandi & Nunes, 2013; Poumadère et al., 2015), and constitute about one third of the ice-free coasts worldwide (Luijendijk et al., 2018). Open sandy beaches constantly evolve in response to multiple environmental drivers occurring on different time scales, making sandy shoreline dynamics strongly sensitive to sea-level rise and wave climate change (Ranasinghe, 2016, 2020). Meanwhile, the expected growth of population density in low-lying coastal areas during the twenty-first century (Merkens et al., 2016; Neuman et al., 2015) increases the need for efficient adaptation plans of coastal communities (Oppenheimer et al., 2019).

The spatial heterogeneity of sea-level rise (SLR), wave-climate change, time scales of adaptation, and vulnerability of coastal communities raises the need for shoreline projections with their related uncertainties that provide full support to risk-informed decision making process (Hinkel et al., 2019; Losada et al., 2019; Toimil et al., 2018, 2020; Wainwright et al., 2015). However, limits in our understanding and modeling capacity of the primary processes driving shoreline change, together with the uncertainties associated to the future climate (e.g., carbon emission scenario, SLR, storminess, etc.), undermine the confidence in future shoreline

estimates proportionally to the time scale of application (Ranasinghe, 2020; Toimil et al., 2020). Many studies focused on the effects of SLR uncertainties (Athanasidou et al., 2020; Le Cozannet et al., 2016, 2019; Thiéblemont et al., 2021; Vousdoukas et al., 2020) and changes in storminess based on data extrapolation and/or empirical models (Allenbach et al., 2015; Casas-Prat et al., 2016; Toimil et al., 2017; Vousdoukas et al., 2020) on future shoreline uncertainties. However, these studies do not explicitly resolve wave-driven shoreline change, and it is advocated that new methods have to be developed to predict the impacts of SLR on the coast (Cooper et al., 2020). Short- and long-term variability in wave energy, as well as the chronology of storm events, can strongly affect future shoreline patterns (Besio et al., 2017; Cagigal et al., 2020; Coco et al., 2014; Dissanayake et al., 2015; Vitousek et al., 2021). Recently, Cagigal et al. (2020) developed and used a stochastic climate-based wave emulator to generate ensembles of wave time series at several beaches, and addressed shoreline response to different wave chronologies. Based on the same emulator, Vitousek et al. (2021) analytically investigated the uncertainties in shoreline predictions associated to the inherent variability of the wave climate in the context of equilibrium shoreline modeling. Kroon et al. (2020) showed the significant effects of wave-climate variability and model uncertainty on the short-term (1 year) probabilistic assessment of coastline change at the Sand Engine (Netherlands). The authors used a one-line model, that is, resolving wave-driven longshore sediment transport gradients and resulting shoreline evolution, as this stretch of coast is longshore transport dominated.

Currently, there are no studies addressing the time evolution of the effects that uncertainties in future SLR and model parameters have on shoreline projections to the end of the 21st century while explicitly resolving wave-driven shoreline response. The recent development of equilibrium shoreline models opened the way to skilful simulation of wave-driven shoreline response on cross-shore transport dominated sites, which are ubiquitous worldwide, on time scales from hours (storm events) to decades, with low computational cost (Antolínez et al., 2019; Davidson et al., 2013; Lemos et al., 2018; Robinet et al., 2018; Splinter, Turner, et al., 2014; Vitousek et al., 2017; Yates et al., 2009). Equilibrium shoreline models are based on the principle that the shoreline dynamically moves toward a time-varying equilibrium condition (Wright & Short, 1984), which can be expressed as a function of the current shoreline position (Yates et al., 2009) or antecedent wave conditions (Davidson et al., 2013). While the two latter equilibrium formulations show similar skill against shoreline observations on a multi-year timescale (Castelle et al., 2014; Montaña et al., 2020), the accuracy of one approach over the other in different wave forcing scenarios is unclear, particularly on long timescales (multi-decadal). In addition, in this type of models, sediment transport processes are described by semi-empirical relationships that require site-specific calibration against observed shoreline data, introducing further uncertainty (D'Anna et al., 2020; Splinter et al., 2013). Implementations of cross-shore equilibrium models into probabilistic frameworks recently showed that uncertainties in the calibration of model free parameters (D'Anna et al., 2020) and in future wave conditions (Vitousek et al., 2021) have a significant impact on model predictions. In addition, recent studies found an inherent connection between the seasonality of wave climate and shoreline model parameters that defines the frequency of shoreline response, for several beaches along the Australian coast (Ibaceta et al., 2020; Splinter et al., 2017).

SLR-driven shoreline retreat is often estimated using the Bruun (1962) model. This model relates the rate of shoreline erosion to the SLR rate and the average slope of the active beach profile, defined between the seaward and landward limits of cross-shore sediment exchange. The seaward limit of the active beach profile is commonly identified by the depth of closure (Hallermeier, 1978). As local scale bathymetric surveys are scarce and the estimation of the depth of closure is essentially empirical, the active beach profile slope is typically associated with large uncertainties (Nicholls, 1998; Ranasinghe et al., 2012).

In this work, we aim at deepening our understanding in the role and impact of different uncertainties in shoreline projections. We perform a global sensitivity analysis (GSA; Saltelli et al., 2008) to unravel the respective contributions of SLR, depth of closure, and shoreline model free parameters uncertainties. The framework is applied to the cross-shore dominated Truc Vert beach (SW France) using two different wave-driven shoreline models, the Bruun model, and state-of-the-art SLR and wave projections for two future representative concentration pathways (RCP) scenarios. The likely range provided along with median SLR estimates in IPCC reports does not cover the full uncertainty range of mean sea level projections. Hence, there remains a probability of up to 33% that sea-level rise exceeds the likely range. Therefore, we also assess shoreline projections in the deterministic high-end SLR scenario, which remains unlikely but

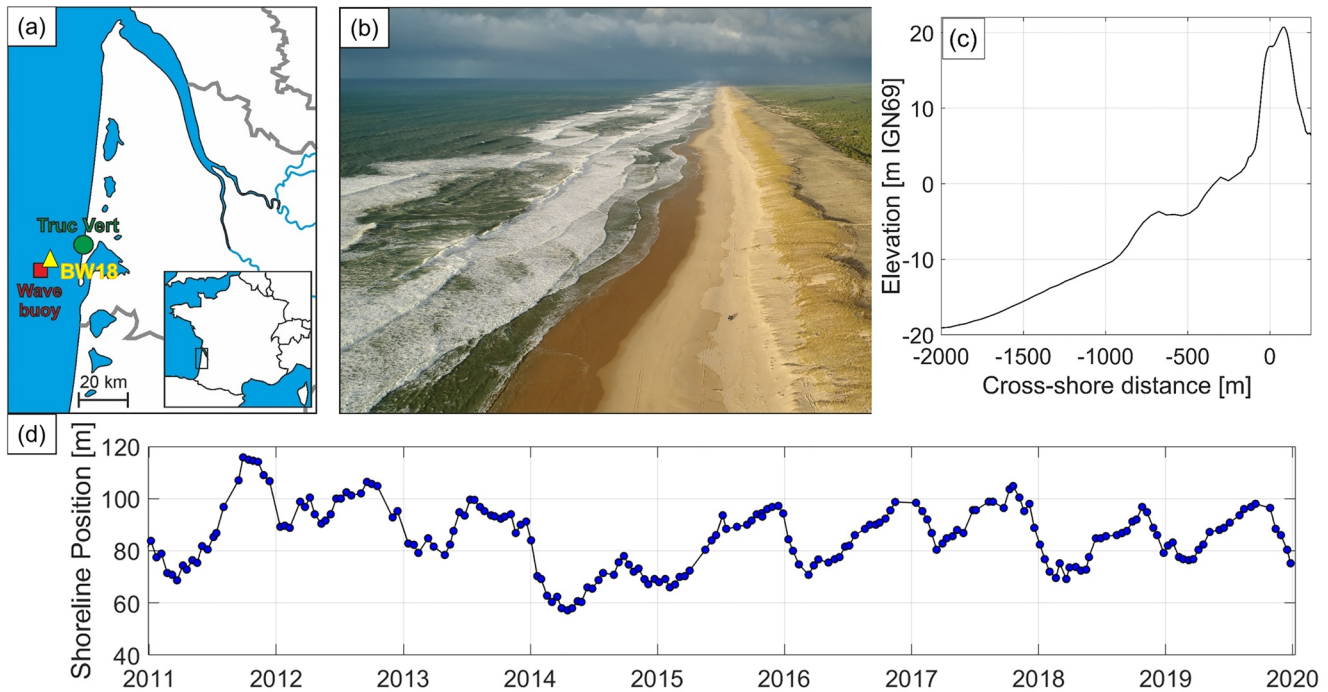


Figure 1. (a) Location of Truc Vert beach (green), wave hindcast grid point co-located with the CANDHIS in situ wave buoy (red), and wave projections grid point (yellow); (b) Picture of Truc Vert beach and dune landscape (photo by V. Marieu); (c) 4 km alongshore-averaged beach-dune profile from merged 2008 topo-bathymetry (submerged beach) and 2018 UAV-photogrammetry digital elevation model (emerged beach and dune); (d) Mean shoreline (1.5-m beach profile elevation proxy) positions between 2011 and 2020 derived from the bimonthly topographic surveys.

plausible and is associated with large impacts (Stammer et al., 2019). The remainder of this paper includes: an outline of Truc Vert beach, the data, the shoreline models, and the method (Section 2); a description of the GSA input variables' probability distributions and the numerical modeling setup (Section 3); and the presentation of the results (Section 4). Discussion and conclusions are provided in Sections 5 and 6, respectively.

2. Study Site, Data and Method

2.1. Truc Vert Beach

Truc Vert is a meso-macrotidal wave dominated sandy beach located in the south of the Gironde coast, southwest France, which extends roughly 100 km between the Gironde river estuary and the south of the Arcachon basin (Figures 1a and 1b). Truc Vert is backed by a high (~20 m) and wide (~250 m) coastal dune system (Robin et al., 2021). The wave climate is characterized by strong seasonal energy fluctuations, and strong interannual winter energy variability (Castelle, Dodet, et al., 2018; Charles et al., 2012; Robinet et al., 2016), the latter associated to large-scale climate patterns of atmospheric variability in the northeast Atlantic region (Castelle et al., 2017). Monthly averaged significant wave height ranges from 1.1 m in August with dominant W-NW direction to 2.4 m in January with dominant W direction. Truc Vert beach has been intensively monitored since 2003 with monthly to bi-monthly topographic DGPS surveys, with additional daily topographic surveys and high-resolution bathymetric surveys collected during the ECORS'08 field campaign (Parisot et al., 2009), see Castelle et al. (2020) for detailed description of the datasets. Since 2017, high-resolution digital elevation model covering 4 km of beach-dune are also derived seasonally from photogrammetry of UAV images (Laporte-Fauret et al., 2019).

The beach morphology is highly dynamic and responds primarily to cross-shore processes driven by the temporal variability of the incident wave climate (Castelle et al., 2014; Robinet et al., 2016, 2018). Overall, this segment of coastline has been observed to be reasonably stable over the past decades (Castelle, Guillot,

et al., 2018), although the interannual distribution of winter wave energy may result in episodic severe beach and dune erosion (Castelle et al., 2015; Masselink et al., 2016).

2.2. Wave Data: Historical and Projections

While a data set of future waves is required to simulate future shoreline change, hindcast wave data were also needed for the present study in order to: (a) run the shoreline models on the past period and estimate the distribution of the model parameters; and (b) support the correction of the wave projection data set.

2.2.1. Hindcast Wave Data (1994–2020)

Historical wave data (H_s , T_p , and D_m), from January 1994 to January 2020, was extracted from the NOR-GAS-UG regional hindcast model (Michaud et al., 2016) at the grid point co-located with the in situ CANDHIS wave buoy (44°39'9"N; −1°26'48"W) moored in ~50 m depth offshore of Truc Vert beach (Figure 1a). The NOR-GAS-UG model covers the French Atlantic coastal area using an unstructured mesh grid with resolution of 10 km offshore, increasing to 200 m nearshore. The wave model was validated against several French and international wave buoy data, and showed 0.96–0.99 correlations coefficients, 0.15–0.21 m RMSE, and −0.02–0.04 m bias (Michaud et al., 2016). The hindcasted wave time series (1994–2020) shows the typical seasonal and interannual modulation of the incident wave climate at Truc Vert beach (Figure 2a).

2.2.2. Future Wave Climate (2020–2100)

Wave-driven shoreline change at cross-shore transport dominated sites is controlled by the variability in incident wave energy including temporal clustering and chronology of storm wave events (Angnuureng et al., 2017; Dissanayake et al., 2015; Splinter, Carley, et al., 2014). Thus, the assessment of future shoreline evolution at Truc Vert requires a continuous wave time series with high resolution (e.g., few hours). Bricheno and Wolf (2018) (hereafter BW18) provide state-of-the-art wave projections throughout the 21st century in the Northeast Atlantic region for the RCP 8.5 and RCP 4.5 scenarios. As part of the Coordinated Ocean Wave Climate Project (COWCLIP), BW18 wave data belong to an ensemble of global and regional wave climate projections, forced with several Global Climate Models and using different wave models. Within COWCLIP, changes were found to be robust in the North Atlantic region, suggesting a slight decrease of annual mean H_s and a clockwise rotation of waves off the Aquitanian coast that is, more pronounced for high climate forcing (Morim et al., 2019). However, amongst the COWCLIP ensemble, to our knowledge, only BW18 produced uninterrupted time series of wave data with sufficient spatial resolution to properly reproduce the wave climate offshore our study site. The continuous hourly time series of wave conditions was produced by BW18 using a dynamical downscaling approach and a nested setup of the WaveWatchIII® spectral wave model (Tolman, 2009). The wave model covers the Northwest European coastal area with a grid resolution of 0.083° (<9 km) and was forced with the downscaled EC-Earth global climate model (Hazeleger et al., 2012). For both RCP scenarios, BW18 model is run from 2006 to 2100 in a regional atmospheric model configuration (~0.11° resolution), in the context of the EURO-CORDEX project. BW18 also provide the results of a *historic* model run, forced with the EC-Earth model climate, for the period 1970–2004. Such simulation is needed to estimate relative change between past and future wave climate or for the correction of the potential biases between the modeling results and reference wave data (e.g., wave buoy data or modeled wave hindcast), which result from climate models bias (see e.g., Charles et al., 2012). From the BW18 modeling, we extracted wave data (H_s , T_p , and D_m) over 2020–2100 (for shoreline projections) from the nearest grid point to the CANDHIS wave buoy (~3 km North-East; Figure 1a), in ~50 m depth, for both RCP 8.5 and RCP 4.5 scenarios. To reduce the bias in modeled future waves, we analyzed the seasonal quantiles of the 1994–2004 portion of BW18 *historic* wave time series (extracted at the same location as the 2020–2100 wave data) and the seasonal quantiles of the NOR-GAS-UG hindcast, and set-up a seasonal *quantile-quantile* correction that we applied to the 2020–2100 wave data set (details in Text S1). The corrected BW18 wave time series for RCP 8.5 and RCP 4.5 scenarios are shown in Figures 2b and 2c, respectively. Hereon, we refer to BW18 as the corrected wave time series.

Here, we adopted $H_s^2 T_p$ (m²s) as a representative variable for deep-water wave energy. The RCP 8.5 and 4.5 2020–2100 wave series show a strong interannual modulation of incident wave energy, which is in line with current wave climate characteristics offshore of Truc Vert. Both scenarios of the BW18 wave projections show several peaks of the 3-months average $H_s^2 T_p$ that are comparable to the 2013–2014 outstanding

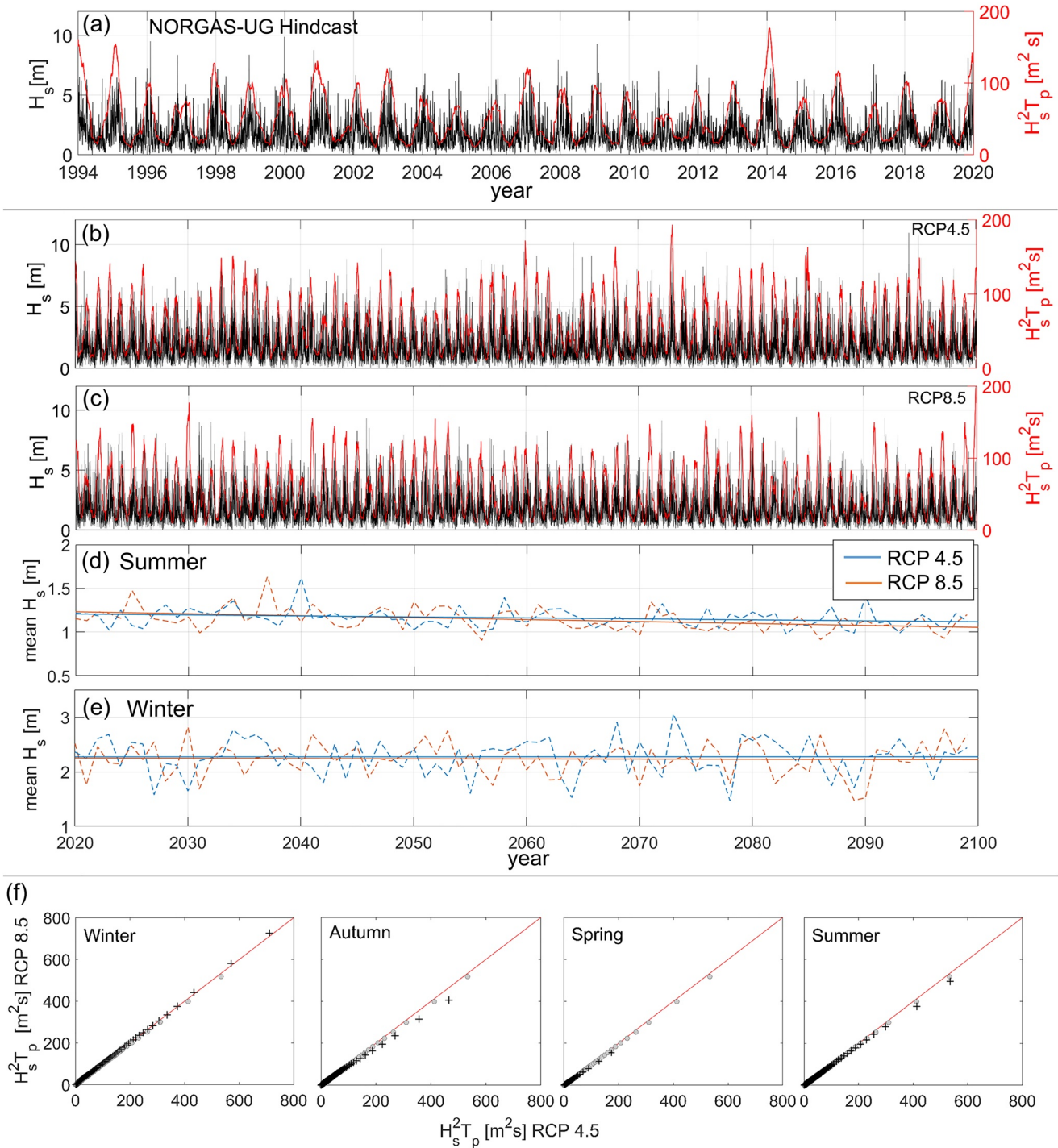


Figure 2. Wave data offshore of Truc Vert, including: time series of H_s (black lines) and 3-months averaged $H_s^2T_p$ (red lines) for (a) the 1994–2020 wave hindcast from NORGAS-UG model ($44^{\circ}39'9''$ N; $-1^{\circ}26'48''$ W), and (b) RCP 8.5 and (c) RCP 4.5 scenarios corrected 2020–2100 Bricheno and Wolf (2018) wave projections; linear trends (solid lines) of annual (d) summer and (e) winter mean H_s (dashed lines) of 2020–2100 corrected Bricheno and Wolf (2018) wave projections, for RCP 4.5 (blue) and RCP 8.5 (orange) scenarios. For RCP 8.5 (RCP 4.5), the trend of summer and winter mean H_s are -2 mm/year (-1 mm/year) and -0.05 mm/year (-0.05 mm/year). These trends were tested to be statistically significant (more than 99% significance) using Student's t-tests. (f) Quantile-quantile comparison between RCP 4.5 and RCP 8.5's 3-months average of $H_s^2T_p$ projections for the four seasons (black crosses) and for the full datasets (gray circles).

high-energy winter ($H_s^2 T_p = 178 \text{ m}^2\text{s}$) experienced at Truc Vert (Figures 2a–2c). For the RCP 8.5 (RCP 4.5) scenario, the projected 3-months average $H_s^2 T_p$ reaches at least 90% of the 2013–2014 peak in 2030, 2080, 2086, and 2099 (2060, 2068, 2073, and 2085; Figures 2b and 2c). While characterized by similar integrated intensity, these winters are preceded by different multi-annual energy trends, with the RCP 8.5 (RCP 4.5) 2080, 2086, and 2099 (2060 and 2068) winters following a positive trend of wave energy (similarly to the 2013–2014 winter), and the 2030 (2060 and 2068) winter following a negative trend of winter energy. Although in both RCP scenarios the incident wave energy fluctuates with a similar interannual period with nearly the same average $H_s^2 T_p$ (52 and 54 m^2s for RCP 8.5 and RCP 4.5, respectively), the RCP 4.5 scenario associates slightly higher energy during Autumn, Summer and Spring (Figure 2f). The 2020–2100 summer mean wave height ($H_{s\text{summer}}$) fluctuates between 0.9 and 1.7 m, with a statistically significant decrease of 2 mm/year (1 mm/year) rates for the RCP 8.5 (RCP 4.5; Figure 2d). Future winter mean wave height ($H_{s\text{winter}}$), which is a key driver of cross-shore wave-dominated shoreline evolution (Dodet et al., 2019), varies between 1.5 and 3 m with a statistically significant decreasing trend under 0.05 mm/year in both RCP scenarios (Figure 2e). This is consistent with previous regional projections (Charles et al., 2012; Perez et al., 2015; Morim et al., 2019).

2.3. Mean Sea Level and Vertical Land Motion

2.3.1. Past Mean Sea Level Reconstruction

As SLR-driven shoreline retreat is explicitly accounted for in the calibration of the shoreline models, past MSL information is required. We reconstructed the geocentric MSL change in the Bay of Biscay over the period 2012–2020 using a Kalman filter approach assimilating available tide gauge records in this region (Rohmer & Le Cozannet, 2019). The resulting SLR rates are roughly constant at $2.1 \pm 0.1 \text{ mm/year}$ (median $\pm \sigma$). Local relative MSL change at Truc Vert beach was calculated by adding the effect of vertical land motion to the relative regional sea level estimate. Vertical land motion in Truc Vert area was estimated using the near Cap-Ferret permanent GNSS station from the SONEL database (Santamaria-Gomez et al., 2017), which provides data from 2005 to 2012, when the station was decommissioned. The GNSS station measures the effects of Glacial Isostatic Adjustment and current gravitational, rotational and deformation changes associated to ongoing glaciers and ice-sheets melting (Frederikse et al., 2020). We subtract their effects from the observed GNSS records over the observation period to assess residual vertical ground motions obtaining a subsidence rate of $1.2 \pm 0.6 \text{ mm/yr}$. This results in a roughly constant SLR rate of $3.3 \pm 0.7 \text{ mm/yr}$ over the past decade (see Figure S5). The observed lowering ground might be due to slow subsidence of the former Leyre riverbed (Klingebiel & Legigan, 1992).

The pointwise Cap-Ferret GNSS station information may not be exactly that of the surrounding area. This is part of the residual uncertainties of our study.

2.3.2. Future Mean Sea Level Projections

State-of-the-art GMSL projections until 2100 are available from the *Special Report of Ocean and Cryosphere in a Changing Climate* (SROCC; Oppenheimer et al., 2019). SROCC estimates build on the *Fifth Assessment Report* (AR5, Wong et al., 2014) with a revised assessment of the Antarctic dynamics contribution based on new evidence on marine ice-sheets instabilities since the AR5. SROCC provides median values of each sea level change contribution with associated *likely range* for several RCP scenarios. Unlike other IPCC reports, the SROCC defines the likely range as the 17th–83rd percentiles of the distribution of sea-level rise (Oppenheimer et al., 2019). We reproduced the SROCC global MSL projections to Truc Vert beach following Thiéblemont et al. (2019) and considering the regional fingerprints of each mechanism contributing to sea-level changes, including the effect of Glacial Isostatic Adjustment (Slangen et al., 2014). This results in regional relative 2020–2100 SLR estimate (median and likely range) of $0.63 \pm 0.26 \text{ m}$ and $0.37 \pm 0.16 \text{ m}$ for the RCP 8.5 and RCP 4.5 scenarios, respectively.

Residual vertical land motion, which is assumed to be due to slow-ongoing geological processes (see subsection 2.3.1 and Klingebiel & Legigan, 1992), is assumed to remain constant ($1.2 \pm 0.6 \text{ mm/yr}$) over the 21st century. Due to the large uncertainty (0.6 mm/yr) of the subsidence rate, the stability of the area is not excluded, but has a very low probability (2.1%). The inclusion of ground motion results in a local relative MSL

rise of 0.73 ± 0.27 m and 0.47 ± 0.17 m from 2020 to 2100 for RCP 8.5 and RCP 4.5 scenarios, respectively (see Figure S5). Further detail on future SLR is provided in Section 3.1.

2.4. Shoreline Change Models

Here, we use two equilibrium-based models to assess wave-driven shoreline response: the Yates et al. (2009) model, and an adaptation of the *ShoreFor* model (Davidson et al., 2013; Splinter, Turner, et al., 2014). As the Truc Vert bathymetry iso-contours are essentially shore-parallel, breaking wave conditions were computed directly from offshore wave conditions using the Larson et al. (2010) formula. Chronic shoreline retreat induced by SLR was estimated using the Bruun (1962) model. As shoreline change at Truc Vert is known to be dominated by cross-shore sediment transport with negligible gradients in longshore transport (Castelle et al., 2014; Splinter, Turner, et al., 2014), we did not compute longshore sediment transport. The following subsections describe the two wave-driven shoreline models and the Bruun model.

2.4.1. Wave-Driven Shoreline Models and Free Parameters

Equilibrium shoreline models are based on the principle that local wave climate drives the shoreline toward a time-varying equilibrium position at a rate that depends on the instantaneous wave thrust (e.g., wave power or energy) available to move the sediment, and the dynamic disequilibrium state of the beach (Wright & Short, 1984). The Yates et al. (2009) model and *ShoreFor* differ primarily in the formulation of the respective disequilibrium conditions.

2.4.1.1. ShoreFor Model

The *ShoreFor* model (hereafter SF) adopts a disequilibrium condition based on the wave history, expressed as a disequilibrium of dimensionless fall velocity ($\Delta\Omega$) and its standard deviation ($\sigma_{\Delta\Omega}$). The governing equation for shoreline change rate reads:

$$\frac{dY}{dt} = k_s^{+/-} P^{0.5} \frac{\Delta\Omega}{\sigma_{\Delta\Omega}} + b \quad (1)$$

where, $k_s^{+/-}$ ($\text{m s}^{-1} \text{W}^{-0.5}$) is a response rate parameter, $P(W)$ is the wave power at breaking, and b (m/s) is a linear term trend. Following Robinet et al. (2018), the disequilibrium term $\Delta\Omega$ at a given time is defined as the difference between the equilibrium dimensionless fall velocity ($\Omega_{\text{eq}}(\Phi)$) and the offshore dimensionless fall velocity (Ω_o), where $\Omega_{\text{eq}}(\Phi)$ is a function of the sediment size, prior wave conditions, and the free parameter Φ . The parameter Φ (days) is a site-specific “beach memory,” and defines the time over which a given wave event has an impact over the equilibrium state of the beach. The $k_s^{+/-}$ parameter is the shoreline response rate, and assumes different values for accretion (k_s^+ , $\Delta\Omega > 0$) and erosion (k_s^- , $\Delta\Omega < 0$) events, which are driven by different processes associating different time scales. The values of the $k_s^{+/-}$ parameter for accretion and erosion conditions are considered proportional through a coefficient r ($k_s^- = r k_s^+$). The r coefficient is not a model free parameter but is defined by the wave forcing, and is such that no trend in wave forcing results in no trend in the modeled shoreline position over the simulated period:

$$r = \frac{\left| \frac{\sum_{i=1}^N \langle F^+ \rangle}{\sum_{i=1}^N \langle F^- \rangle} \right|}{\left| \frac{\sum_{i=1}^N \langle F^+ \rangle}{\sum_{i=1}^N \langle F^- \rangle} \right|} \quad (2)$$

$$F = P^{0.5} \frac{\Delta\Omega(\Phi)}{\sigma_{\Delta\Omega}} \quad (3)$$

where N is the full length of the simulated period, F^+ and F^- are the forcing during accretion ($\Delta\Omega > 0$) and erosion ($\Delta\Omega < 0$) events, respectively, and $\langle \cdot \rangle$ denotes an operation that removes the linear trend. Here, the sign of $\Delta\Omega$ does not change the absolute value of $F^{+/-}$. For an extended description of SF the reader is referred to Davidson et al. (2013) and Splinter, Turner, et al. (2014). In SF, the model free parameters to be calibrated at a given site are k_s^+ , Φ and b . Physically, the $k_s^{+/-}$ ($\text{m s}^{-1} \text{W}^{-0.5}$) is a measure of the efficiency of wave forcing to drive shoreline change (as described by Splinter, Turner, et al., 2014), which can also be interpreted as a time scale of shoreline response (Vitousek et al., 2021). Indeed, a low efficiency corresponds

to a slow shoreline response and a longer time scale, and vice versa. $\Phi(\text{days})$ is a time scale for the duration of the impact that past waves exerted on the beach, and provides the ability for the model equilibrium condition to evolve along with long-term wave energy trends. The parameter $b(\text{m/s})$ is a linear term that encapsulates the effect of slow processes, other than wave-driven equilibrium based, which may drive chronic shoreline change (e.g., wind driven sediment transport) and that are not explicitly resolved in the model. We note here that, while accounting for the effects of slow processes using a constant linear trend (i.e., b) can improve the model skill for simulated periods within the decade, the application of such trend over longer time scales (decades to centuries) becomes increasingly inaccurate (D'Anna et al., 2020). Therefore, given the long time scale of our application and the absence of secondary processes (e.g., longshore gradients in sediment transport) that may drive long-term shoreline trends at Truc Vert, we set $b = 0$.

2.4.1.2. Yates Model

In Yates' model (hereafter Y09) the disequilibrium condition is defined as a function of the current shoreline position, and the cross-shore rate of shoreline change is calculated as follows:

$$\frac{dY}{dt} = k_y^{+/-} E^{0.5} (E_{eq}(Y) - E) \quad (4)$$

where E (m^2) is the wave energy, $k_y^{+/-}$ ($\text{m}^2 \text{s}^{-1}/\text{m}$) is the response rate parameter, $Y(\text{m})$ is the present shoreline position, and $E_{eq}(Y)$ is the wave energy in equilibrium with the current shoreline position Y through a linear relationship:

$$E_{eq}(Y) = a_1 Y + a_2 \quad (5)$$

where a_1 (m^2/m) and a_2 (m^2) are free model parameters. The $k_y^{+/-}$ parameter is analogous to $k_s^{+/-}$ of SF in that it represents the efficiency rate of the incident wave forcing to shoreline change, or a time scale parameter (see the analytical derivation of the Y09 time scale of shoreline response in Vitousek et al., 2021). In the Y09 model no assumption is made on a possible relationship between the k_y^+ and k_y^- , which are both considered model free parameters and, as well as a_1 and a_2 , require specific calibration for each field site application. Contrarily to SF, here the equilibrium state formulation (Equation 5) does not depend on recent wave conditions, making this model insensitive to wave-climate variability on timescales longer than the calibration period. Instead, Equation 5 depends on the current shoreline position (Y), introducing the potential for feedbacks between Y09 and shoreline change induced by other cross-shore processes (e.g., SLR). Herein, such processes are resolved independently and linearly superposed, so that no feedback is enabled. Physically, $k_y^{+/-}$, once again is a measure of the shoreline reactivity to the incident wave forcing, and is expressed in ($\text{m} \text{s}^{-1}/\text{m}$). Although the dimensions of a_1 and a_2 are “energy/meter” and “energy,” respectively, the role of these parameters in the model is purely empirical. A rearrangement of the terms in Equations 2 and 3 results in combinations of model parameters that are representative of equilibrium time and spatial scales (Vitousek et al., 2021). However, here we use Y09 in its original form, where a_1 and a_2 are treated as empirical parameters.

2.4.2. Sea-Level Driven Shoreline Recession

We include SLR-driven shoreline recession using the Bruun (1962) model, which is based on the equilibrium beach concept and cross-shore balance of sediment volume. While the reliability of this model is highly debated for its oversimplification of the reality (Cooper & Pilkey, 2004; Ranasinghe et al., 2012), its simple linear formulation has been extensively used worldwide. In addition, Truc Vert beach is a relatively undisturbed beach-dune environment with large accommodation space, which makes this sites in line with most of the Bruun Rule underlying assumptions. The Bruun model assumes that under rising sea level, on time scales larger than years, the average beach profile translates upwards and landwards. The resulting shoreline retreat (dY_{SLR}/dt) depends on SLR and the average slope of the active beach profile, here extending from the dune crest down to the depth of closure (DoC), defined as the depth beyond which sediment exchange is considered negligible (Bruun, 1988; Wolinsky & Murray, 2009):

$$\frac{dY_{\text{SLR}}}{dt} = \frac{\text{SLR}_{\text{rate}}}{\tan\beta} \quad (6)$$

where SLR_{rate} is the rate of SLR (m/time), and $\tan\beta$ is the average profile slope defined between the DoC and the dune crest. We estimated the DoC according to Hallermeier (1978), and the corresponding $\tan\beta = 0.023$ using the beach profile reported in Figure 1c.

2.5. Global Sensitivity Analysis

Numerical modeling of shoreline change inherits the uncertainties associated to input variables and their complex interactions, affecting the robustness of the shoreline projections. While numerical modeling provides a “key-hole” to observe the explicit interactions among defined sets of variables, sensitivity analysis provides a way to understand the role of input variables uncertainties in shoreline predictions. Here, we use the framework proposed by D’Anna et al. (2020), who used a variance-based Global Sensitivity Analysis (GSA; Saltelli et al., 2008; Sobol’, 2001) to investigate the relative contributions of the uncertainties affecting input variables to the uncertainties of modeled shoreline predictions, and their evolution in time. The method consists in propagating the input uncertainties through the model obtaining a probabilistic estimate of the shoreline projections, and performing a GSA which decomposes the variance of model results into several contributions, each one associated with an input variable. Each of these contributions is used to estimate a measure of the model results sensitivity to the input uncertainties with a sensitivity index known as *first-order Sobol’ index* (S_i). The S_i (0–1) quantifies the ratio of output’s variance associated with the uncertainties of a given input X_i , that is, the reduction in the output variance that would occur if the uncertain input X_i was set to its true value, and is defined as:

$$S_i = \frac{\text{Var}\left(E\left(Y|X_i\right)\right)}{\text{Var}\left(Y\right)} \quad (7)$$

where Var is the variance operator, E is the expectation operator, Y is the modeled shoreline position, and X_i is the i -th uncertain input variable. Further details on GSA and S_i are provided in Text S3.

Here, we address the relative impact of uncertainties associated to SLR, DoC, and of model free parameters on shoreline projections (Y) and their evolution in time for the two different modeling approaches described in Section 2.4. Identifying the main source of model results uncertainties through time is a fundamental step toward improving the reliability of long-term shoreline projections. Following D’Anna et al. (2020), we computed the S_i s using the modularized sample-based approach by Li and Mahadevan (2016), which allows accounting for the statistical dependence between model free parameters, and we estimate S_i s for the purpose of “Factors’ Prioritization” (as defined by Saltelli et al., 2008). At a given time, the Factors’ Prioritization identifies the main driver of model results uncertainty (associating the largest S_i), that is, the uncertain input variable that would most reduce the output’s variance when fixed to its true value. The method can be summarized in three steps:

1. Definition of probability distribution associated to each stochastic input variable (SLR, DoC and model free parameters);
2. Generation of ensemble modeled shoreline projections, by means of a Monte-Carlo-based procedure (with accounts for dependence among the input parameters); and
3. Computation of first-order Sobol’ index time series for each uncertain input variable.

The GSA results are interpreted as the repartition of the variance of shoreline projections into normalized portions (between 0 and 1) imputed to the uncertain input variables. For instance, at a given time, $S_{i,\text{SLR}} = 0.3$ means that uncertainties in future SLR alone are responsible for 30% of the variance in shoreline projections. However, the magnitude of a S_i alone is not sufficient to identify the main driver of the shoreline projections’ variance, which is defined by comparing the values of S_i for all input variables and ranking them in terms of importance.

Figure 3 synthesizes the generalized method and details for the Truc Vert probabilistic applications (excluding the additional high-end SLR deterministic scenario).

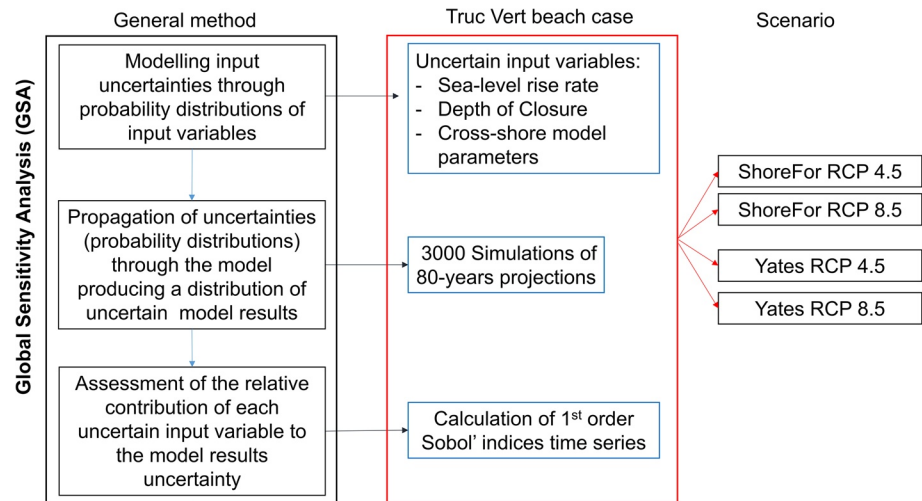


Figure 3. Flowchart of the method applied herein, summarized for a general case (black box), and for the Truc Vert application (red box) in the four application scenarios.

3. Input Probability Distributions for Future Projections

3.1. Probabilistic Sea-Level Rise

Sea-level projections inherit uncertainties associated with physical unknowns and modeling of the contributing processes. While many efforts were dedicated to assess such uncertainties, there is no single approach to define MSL probability distributions yet (Jackson & Jevrejeva, 2016; Jevrejeva et al., 2019; Kopp et al., 2014). We produced probabilistic relative MSL projections, conditional to the RCP 8.5 and 4.5 scenarios, defining time varying normal probability distributions characterized by the yearly median and standard deviations obtained in Section 2.3.2 (Figures 4a and 4b), following Hunter et al. (2013). In the high-emission scenario (RCP 8.5), the large uncertainty associated with Antarctic ice sheet dynamics generates a skewness of the distributions in the second half of the 21st century, enhancing the amount of possible extreme SLR (Grinsted et al., 2015; Jackson & Jevrejeva, 2016; Kopp et al., 2014). The upper tail of the skewed probability distribution is very much debated (Jevrejeva et al., 2019) and is not represented by the Gaussian distributions. Therefore, in addition to the Gaussian distribution reflecting the SROCC assessment (Oppenheimer et al., 2019), we consider a high-impact, low probability high-end sea level scenario that might take place for high greenhouse gas emissions (RCP 8.5; black line in Figure 4b) following the same assumptions as Thiéblemont et al. (2019) (see Text S2).

The possibility that the subsidence rate revealed by the Cap-Ferret GPS station is not representative of the Truc Vert area (located at 8 km distance) constitutes a residual uncertainty that cannot be quantified, and is not accounted in this study due to the lack of quantitative information supporting an alternative scenario for residual vertical ground motions.

3.2. Depth of Closure

The active beach profile slope is critical to SLR-driven erosion rate (Section 2.4), and strongly depends on the depth of closure (DoC). The DoC was calculated from the wave climate using the Hallermeier (1978) formula. Given that DoC depends on the period of time over which the Hallermeier formula is applied (Nicholls, 1998), we iteratively applied the Hallermeier formula over a 1-year moving window of the future wave climate with a 30-days step. For both RCP 8.5 and RCP 4.5 scenarios, the latter procedure generated an ensemble of possible DoC values well fitted by a Gaussian distribution (Figure 4c). The DoC probability distribution shows higher median and standard deviation values in the RCP 4.5 ($\mu = 17.2$ m; $\sigma = 1.75$ m) than in the RCP 8.5 ($\mu = 16.3$ m; $\sigma = 0.95$ m). This results from the more frequent occurrence and larger wave heights associated to isolated extreme events in the RCP 4.5 scenario, compared to the RCP 8.5 scenario.

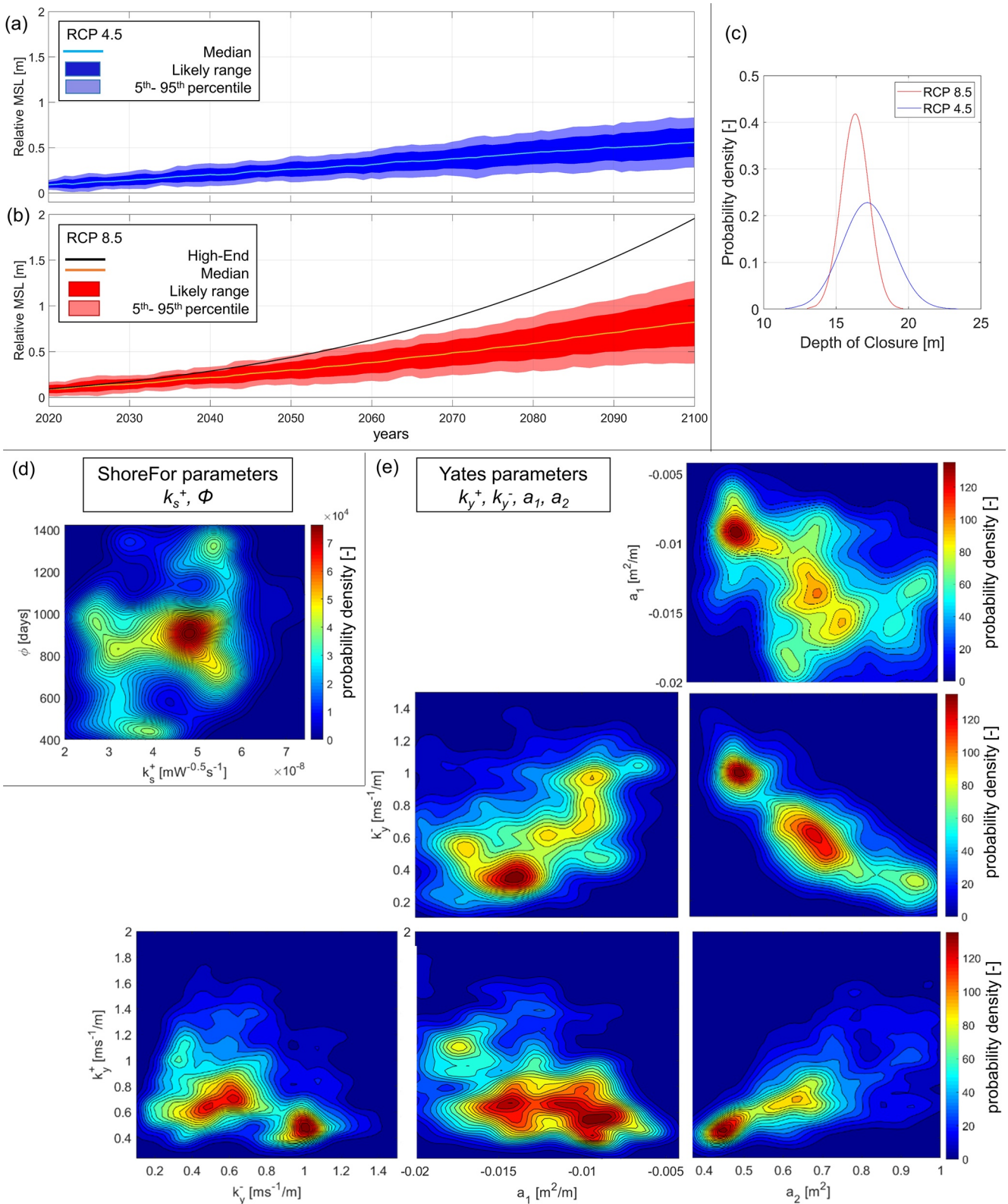


Figure 4.

Table 1
Optimized Combinations of Cross-Shore Model Free Parameters, and Respective Range of Variation in the Probability Distributions

Model	Model parameter	Optimized value	Distribution range
ShoreFor	k_s^+ [$m^{1.5} s^{-1} W^{0.5}$]	4.4×10^{-8}	$[2; 7.4] \times 10^{-8}$
	Φ [days]	1,193	[400; 1,423]
Yates	k_y^+ [$m^2 s^{-1}/m$]	0.87	[0.24; 2]
	k_y^- [$m^2 s^{-1}/m$]	0.5	[0.1; 1.5]
	a_1 [m^2/m]	-0.008	[-0.02; -0.004]
	a_2 [m^2]	0.49	[0.33; 1]

3.3. Model Parameters

Numerical models are associated with uncertainties owing to the choice of modeling approach and to the estimation of model free parameters. We accounted for the uncertainty conditional to the choice of modeling approach assessing the shoreline projections using the Y09 and the SF models described in Section 2.4.1, in two separated scenarios. Both models rely on shoreline observations to calibrate the respective free parameters, and inherit uncertainties due to the quality and amount of available data (Splinter et al., 2013), to possible non-stationarity of the parameters in respect to the wave climate (Ibaceta et al., 2020), and to the optimization method. Uncertainties affecting model free parameters of the Y09 model ($k_y^{+/-}$, a_1 , and a_2) and the SF model (k_s^+ , Φ) are synthesized by their associated joint probability distribution. We follow the approach developed in D'Anna et al. (2020), who calibrated the SF model free parameters

using the Simulated Annealing algorithm (Bertsimas & Tsitsiklis, 1993), and determined their joint probability distribution by fitting an empirical multivariate distribution (multivariate kernel function) on an ensemble of model parameters combinations. The authors built the latter ensemble selecting all parameters combinations that produced a RMSE <10 m against observed shoreline data during the optimization process. Unlike D'Anna et al. (2020), here we calibrated the models between January 2012 and December 2019, where no long-term trend in shoreline position is observed, in line with the assumption of the SF parameter $b = 0$ (see Section 2.4.1). In addition, we used the Nash-Sutcliffe (Nash & Sutcliffe, 1970) efficiency score (NS) instead of the RMSE to determine the models' performance (as for instance in Kroon et al., 2020). The NS measures the model skill in comparison to the "mean model" (defined as the observed mean shoreline position), based on the error's variance, and it is calculated as follows:

$$NS = 1 - \frac{\sum_{n=1}^N (Y_m^n - Y_o^n)^2}{\sum_{n=1}^N (\bar{Y}_o - Y_o^n)^2} \quad (8)$$

where N is the number of observations, Y_m^n and Y_o^n are the n -th modeled and observed shoreline positions, respectively, and \bar{Y}_o is the mean of the observed shoreline positions. The NS coefficient can range between $-\infty$ and 1, where $NS = 1$ corresponds to a model perfectly reproducing the observations, $NS = 0$ to a model with skill comparable to the "mean model", and $NS < 0$ corresponds to models less skilful than the "mean model". We obtained the probability distribution using combinations of parameters that resulted in a $NS \geq 0.25$ (compared to the maximum $NS = 0.63$), which corresponds to a max RMSE of ~ 10 m consistently with D'Anna et al. (2020). We defined the latter threshold with the iterative procedure described in Text S4. This procedure results in the probability distributions of $k_y^{+/-}$, a_1 , and a_2 for Y09, and k_s^+ and Φ for SF shown in Figures 4d and 4e, with the range of possible parameters values reported in Table 1.

3.4. Model Setup of Shoreline Projections

Four ensembles of 3,000 possible shoreline trajectories from 2020 to 2100 were generated using the SF and Y09 shoreline change models, and the Bruun Rule, for the two RCP 8.5 and RCP 4.5 scenarios (Table 2). Wave-driven shoreline response (short-term) and SLR (long-term) were computed individually and then linearly combined, so that no feedback mechanisms occur between the models, in line with previous applications (D'Anna et al., 2020; Vitousek et al., 2017).

Figure 4. Probability distributions of: relative mean sea level over the period 2020–2100, including the likely (dark shaded areas) and 5–95th percentile (light shaded areas) ranges, for (a) RCP 4.5 and (b) RCP 8.5 scenarios, with deterministic high-end sea-level projections based on 2100 high-end "highest-modeled" estimates following Thiéblemont et al. (2019) (black line); (c) Gaussian distributions of depth of closure values calculated over the 2020–2100 wave time series for RCP 4.5 (blue curve) and RCP 8.5 (red curve) scenarios; and empirical joint probability distributions of (d) ShoreFor [k_s^+ , Φ] parameters, and (e) Yates [$k_y^{+/-}$, a_1 , and a_2] parameters, obtained fitting a kernel density function (with bandwidths estimated from the marginal kernel density function for each variable) on 6,000 combinations of model parameters producing $NS > 0.25$ against shoreline data.

Table 2

Probabilistic Future Scenarios for Two Representative Concentration Pathways (RCP) and Two Different Wave-Driven Modeling Approaches, Using the Bruun Rule and 3,000 Different Combinations of Model Parameters, SLR Percentile and DoC

Future scenario	SLR-driven shoreline change	Wave-driven shoreline change	# Combinations of uncertain variables
RCP 4.5	Bruun Rule	<i>ShoreFor</i> (SF)	3,000
		<i>Yates</i> (Y09)	3,000
RCP 8.5	Bruun Rule	<i>ShoreFor</i> (SF)	3,000
		<i>Yates</i> (Y09)	3,000

Abbreviation: SLR, sea-level rise.

For each model and RCP scenario, 3,000 simulations were run with different combinations of model free parameters, DoC and SLR time series, sampled from the respective probability distributions. Shoreline change was computed with a 3-h time step from the January 1, 2020 to the December 31, 2099 starting from the same shoreline position ($Y_0 = 0$), and model outputs were recorded with a 2-weeks resolution. As the characteristics of the MSL probability distribution are time-dependent, we randomly sampled percentile values and extracted the corresponding MSL at each year. The ensemble projections character was synthesized by the *likely range*, defined here at each time step as the variance, and the *envelope* (min and max) of modeled shoreline positions, acknowledging that the latter is dependent on the number of simulations and the tails of the probability distributions. The impact of individual winters on shoreline projections is qualitatively discussed observing the distributions of shoreline positions corresponding to the most seaward and landward median shoreline position within each simulated annual cycle (September 1–31,

August). We analyzed the decadal shoreline trends by filtering the modeled shoreline time series with a 5-years running mean. In addition, for RCP 8.5 scenario, a deterministic high-end-SLR simulation was run with both shoreline models using the optimized model parameters (Table 1) and the median DoC. It is to be noted that the GSA results (i.e., S_s) are calculated on the likely range (variance) of the model results, regardless of the envelope of modeled shoreline positions.

4. Results

4.1. Shoreline Projections

The four future scenarios in Table 2 resulted each one in 3,000 shoreline evolution simulations spanning 2020–2100 (Figures 5 and 6). Figures 5c, 5d and 6c, 6d represent the distribution of 3,000 modeled shoreline positions at each recorded output time. All scenarios show a net erosion by 2100, mostly driven by SLR (Table 3). All model ensembles also show large interannual variability that is, essentially enforced by the interannual variability in incident winter-mean wave height (Figures 5a and 5b and 6a and 6b). In the RCP 8.5 (RCP 4.5) scenario we observe a long-term shoreline change pattern responding to alternating sequences of high- and low-energy winters with a period of ~20 years (~10 years) and even longer (Figures 5a, 5e, 5f and 6a, 6e, 6f).

Figures 5c and 5d (Figures 6c and 6d) show several episodes of rapid erosion driven by isolated extreme energy winters, for instance for the RCP 8.5 (RCP 4.5) scenario in winter 2030, 2076, and 2086 (2068, 2073, and 2085). The two wave-driven shoreline models (Y09 and SF) produce consistent short- and long-term shoreline cycles, with larger tendency to accretion in SF than in Y09 during extended periods of low energy winters, for instance during 2050–2055 for RCP 4.5 and 2060–2070 for RCP 8.5 (Figures 5a, 5e, and 5f and 6a, 6e, and 6f).

In the RCP 4.5 emission scenario, the modeled 2020–2100 Truc Vert shoreline trend leads to a likely (envelope) retreat of 15–33 m (4–75 m) with Y09, and 10–23 m (6–65 m) with SF. On a yearly time scale, the shoreline position is likely (envelope) to be farther landward from the initial position, by 76 m (123 m) with Y09, and 43 m (74 m) with SF (Figures 5c and 5d, Table 3). Indeed, the occurrence of extreme winters can produce significant landward shifts of the envelope of shoreline positions, as observed during the 2084–2085 winter (Figures 5c and 5d).

When forced with RCP 8.5 scenario's wave and MSL projections, from 2020 to 2100 simulations indicate an average likely (envelope) erosion of 27–48 m (16–83 m) using Y09, and 14–33 m (2–67 m) using SF (Figures 6d and 6e). In this scenario, over the simulated period the likely (envelope) most landward shoreline position reaches up to 70 m (108 m) from the initial shoreline position with Y09 model, and 48 m (76 m) with SF (Figures 6c and 6d, Table 3). Similarly to the RCP 4.5, here we observe for both models some important shifts in shoreline position distribution owing to extreme winters such as 2086s winter (Figures 6c and 6d).

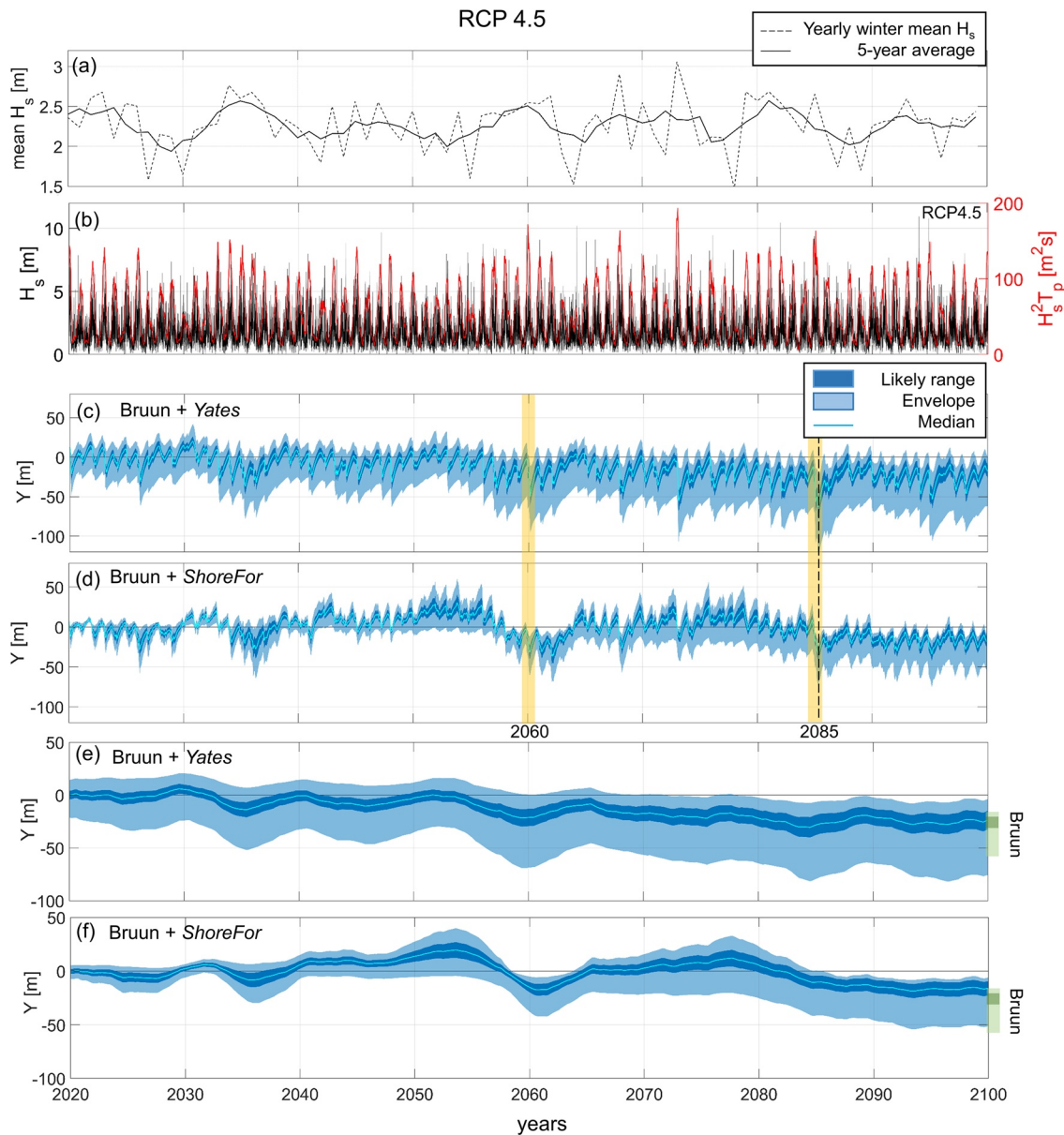


Figure 5. (a) Time series of winter mean wave height of the BW18 RCP 4.5 projections (dashed line) with corresponding 5-years average (solid line); (b) BW18 RCP 4.5 wave height time series (black line), and 3-months average $H_s^2 T_p$ time series (red line); RCP 4.5 scenario 2020–2100 shoreline projections at 14-days resolution obtained using (c) Y09 and (d) SF; and 5-years running mean shoreline projections modeled with (e) Y09, (f) SF, and the standalone Bruun Rule (green bars). Dark (light) blue shaded areas indicate the likely (envelope) range, that is, variance (min-max), of shoreline position, and solid light line median shoreline position. The dashed vertical line indicates the most landward shoreline position over the simulated period. Yellow shaded areas indicate examples of years including high-energy winters.

In the high-end SLR scenario, both models predict a shoreline position within the envelope of probabilistic projections until 2090, before the shoreline moves further inland during the last decade (Figures 6d and 6e). The modeled 5-years averaged shoreline position in 2100 is of 88 and 74 m for Y09 and SF, respectively (Table 3). The most landward shoreline position observed throughout the simulation is 107 m with Y09, and 86 m with SF (black dashed line in Figures 6c and d).

The likely (envelope) ranges erosion produced by the combined Y09+Bruun models at the end of the simulated period are comparable (larger) to the standalone application of the Bruun Rule (Table 3, and in Figures 5 and 6e, 6f with Bruun model predictions in green). With the combined SF + Bruun models, the likely (envelope) ranges of shoreline positions obtained show ~10 m (~15 m) less erosion than the Bruun Rule.

Table 3

Likely (Modeled Shoreline Variance) and Envelope (Min-Max) Values of the 5-Years Averaged Projected Shoreline Position in 2100, and 2020–2100 Most Landward Shoreline Position, Obtained Using the Standalone Bruun Rule (B), and the Combined B With Y09 and SF Equilibrium Shoreline Models, for the RCP 4.5 and RCP 8.5 Probabilistic Scenarios, and the Deterministic High-End SLR Scenario

Scenario	2100 5-years averaged shoreline position		Most landward shoreline position		
	likely range (m)	envelope (m)	likely (m)	envelope (m)	
RCP 4.5	Y09 + B	−15--33	−4--75	−76	−123
	SF + B	−10--23	−6--52	−43	−74
	B	−21--33	−17--60	−33	−60
RCP 8.5	Y09 + B	−27--48	−16--83	−70	−108
	SF + B	−14--33	−2--65	−48	−76
	B	−28--49	−21--86	−49	−86
Deterministic scenario	2100 5-years averaged shoreline position (m)		Most landward shoreline position (m)		
High-end RCP 8.5	Y09 + B	−95	−111		
	SF + B	−74	−84		
	B	−81	−81		

Abbreviation: SLR, sea-level rise.

4.2. Global Sensitivity Analysis

In both RCP 8.5 and 4.5 scenarios and for both shoreline model applications, the GSA shows that over the first 30 years of simulation the variance of modeled shoreline projections is driven primarily by the uncertainties in model free parameters, while the effects of SLR uncertainties on shoreline position become increasingly significant after 2050 (Figures 7 and 8). The S_i s of the Y09 and SF response rate parameters ($k_y^{+/-}$ and k_s^+ , respectively) and the SF beach memory parameter (Φ) show seasonal (6 months) and decadal modulation with a decreasing trend as shoreline projections become more sensitive to SLR (Figures 7c and 7d and 8c and 8d). Variations in $k_y^{+/-}$ and k_s^+ are the primary source of shoreline projection uncertainties during accretion periods. However, the response rate parameters' uncertainties have a stronger impact on seasonal scale when using the Y09 model (Figure 7c), and a larger impact on interannual scale when using the SF model (Figure 8c), due to the different response of the models to incident wave energy variability. Seasonal modulation is also observed for the S_i s of the Y09 empirical parameters (a_1 and a_2), although the correlation between the variability in incident wave conditions and the parameters' S_i s, (both filtered of their seasonal signal with a 1-year running mean) is negligible ($R^2 = \sim 0.06$ for a_1 , and $R^2 = \sim 0.03$ for a_2). However, the estimated a_1 's and a_2 's S_i s remain below 20% during most of the simulated period with occasional peaks up to 45% (Figures 7e and 7f). The primary effects of SLR uncertainties emerge at different times, which depend both on the RCP scenario and on the shoreline model. When using Y09, a positive trend in SLR's S_i emerges in the 2050–2060 period, with SLR's S_i exceeding those of model parameters since approximately 2060–2070, for both RCP scenarios (Figure 7g). Instead, with SF in the RCP 8.5 (RCP 4.5) scenario, such quasi-monotonic trend appears later, approximately during the 2070s (2060s) and only exceeds the model parameters' S_i s after 2085 (2080; Figure 8e). For all scenarios, DoC's S_i slowly increases, with similar trends as SLR's S_i , and reaches approximately 5% and 10%, in the RCP 8.5 and 4.5 scenarios, respectively. This difference is probably due to the larger uncertainties of SLR in the RCP 8.5 scenario (Figure 4b), and to the larger variance of the DoC probability distribution obtained for the RCP 4.5 scenario (Figure 4c).

5. Discussion

5.1. Sea-Level Rise

While observed shoreline erosion in Aquitaine is not yet attributed to SLR, sooner or later a SLR-driven signal will emerge from the current shoreline change variability, as sea levels are committed to rise by meters over the coming centuries (T. R. Anderson et al., 2015; Oppenheimer et al., 2019). Our results suggest that

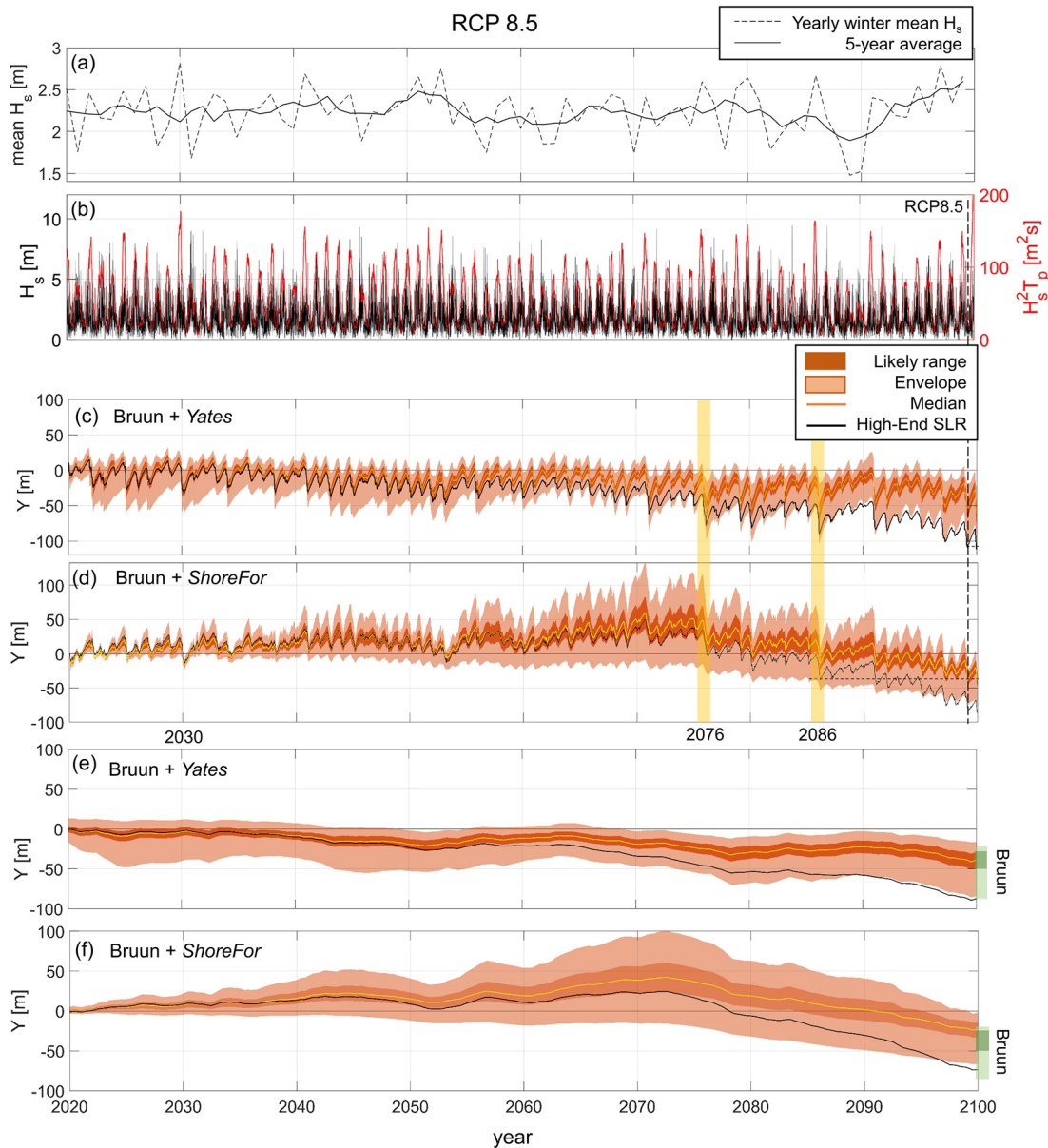


Figure 6. (a) Time series of winter mean wave height of the BW18 RCP 8.5 projections (dashed line) with corresponding 5-years average (solid line); (b) BW18 RCP 8.5 wave height time series (black line), and 3-months average $H_s^2 T_p$ time series (red line); RCP 8.5 scenario 2020–2100 shoreline projections at 14-days resolution obtained using (c) Y09 and (d) SF; and 5-years running mean shoreline projections modeled with (e) Y09, (f) SF, and the standalone Bruun Rule (green bars). Dark (light) shaded areas indicate the likely (envelope) range, that is, variance (min-max), of shoreline position. Black solid lines indicate shoreline projections in the RCP 8.5 high-end sea-level rise (SLR) scenario. The dashed vertical line indicates the most landward shoreline position over the simulated period. Yellow shaded areas indicate examples of years including high-energy winters.

these times of emergence of a SLR-driven erosive trend could be visible during the second half of the 21st century, possibly by 2070. This is consistent with the fact that uncertainty (17–83th percentiles) in future sea level grows from roughly 15 cm by the mid 21st century to 30 cm (RCP 4.5) and 50 cm (RCP 8.5) in 2100. Yet, this result relies on our modeling assumptions, including the Bruun Rule and the *Yates* or *ShoreFor* models.

The GSA applications to four simulated scenarios indicate that uncertainties in the modeled 2020–2100 shoreline projections at Truc Vert are primarily caused by uncertainties in model free parameters between the present day and 2050. The effects SLR uncertainties always emerge as a significant contribution to the shoreline change uncertainties in the second half of the century. We also observed that the time evolution

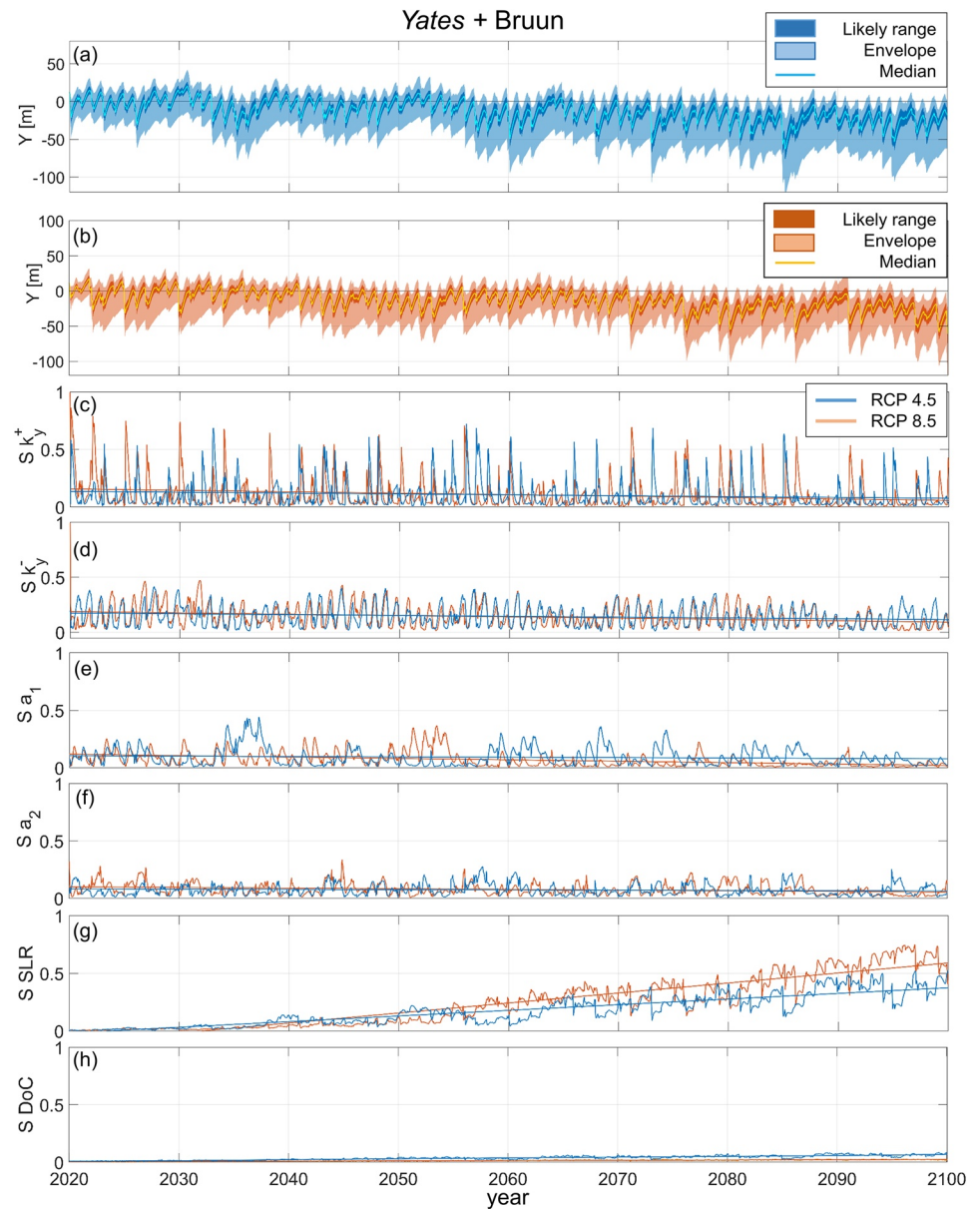


Figure 7. Global Sensitivity Analysis results over the period 2020–2100 using the *Yates* model in the RCP 4.5 (blue lines) and RCP 8.5 (orange lines) scenarios. (a) RCP 4.5 and (b) RCP 8.5 Ensemble shoreline projections (shaded areas) over 2020–2100; First-order Sobol' index time series for (c) k_y^+ , (d) k_y^- , (e) a_1 , (f) a_2 , (g) sea-level rise, and (h) depth of closure, with respective linear fit (solid straight lines).

of S_j s and the onset of SLR uncertainties effects are conditional to the RCP scenario (in agreement with Le Cozannet et al., 2019), the choice of shoreline model, and the variability of forcing wave climate.

The shoreline trajectory obtained in the deterministic high-end SLR scenario exceeds the envelope of probabilistic projections in the last simulated decade. Truc Vert beach is remote and backed by a high (~20 m) and wide (~250 m) dune system, so that shoreline retreat is not limited by non-erodible geological outcrops or coastal structure. While such large erosion does not threaten any human assets close to Truc Vert beach, such scenario, though unlikely, questions adaptation planning in other eroding urbanized coastal areas with limited accommodation space in southwest France.

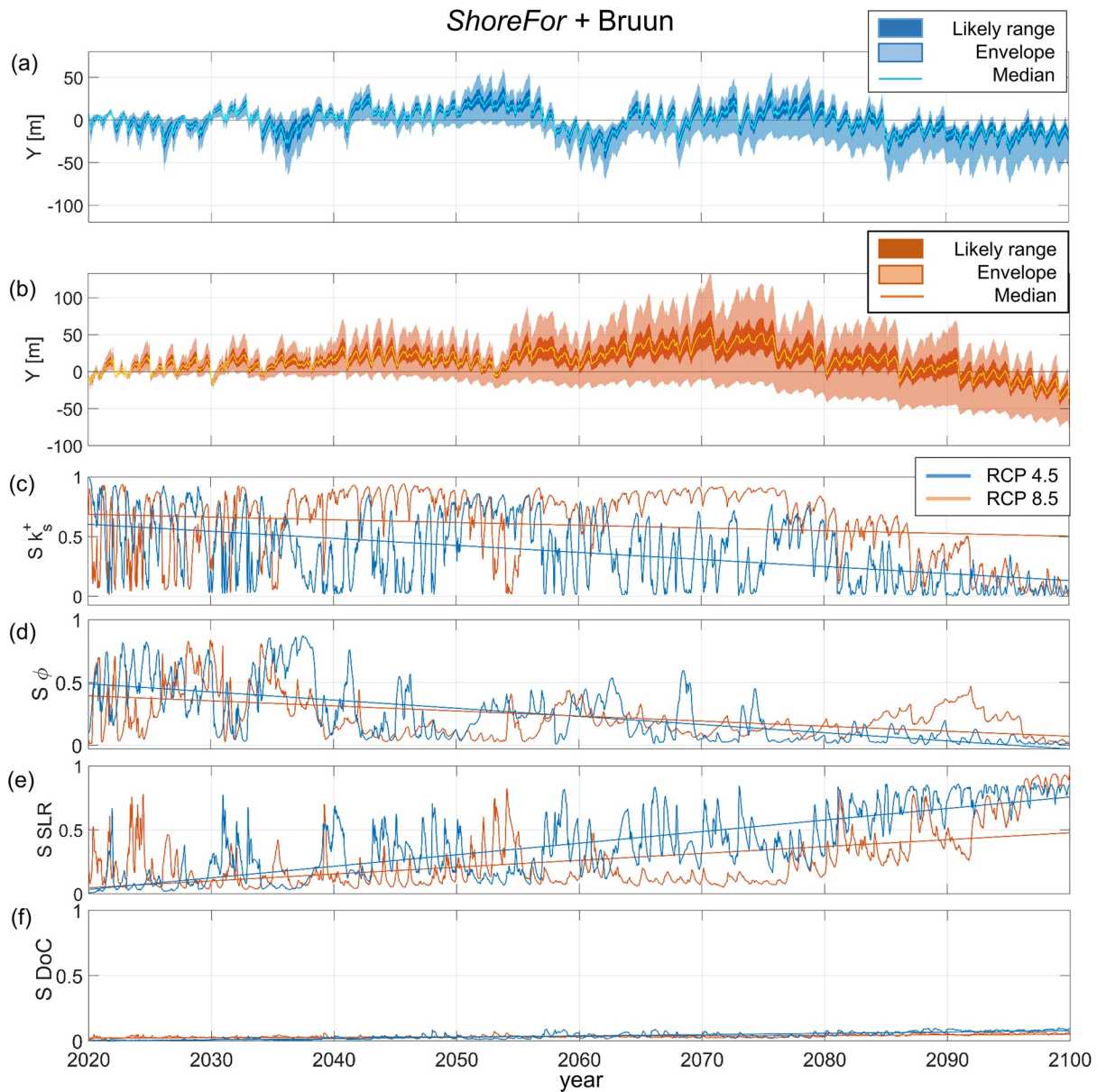


Figure 8. Global Sensitivity Analysis results over the period 2020–2100 using the *ShoreFor* model in the RCP 4.5 (blue lines) and RCP 8.5 (orange lines) scenarios. (a) RCP 4.5 and (b) RCP 8.5 Ensemble shoreline projections (shaded areas) over 2020–2100; First-order Sobol' index time series for (c) k_s^+ , (d) Φ , (e) sea-level rise, and (f) depth of closure, with respective linear fit (solid straight lines).

5.2. Shoreline Models

While the SF and Y09 models are both based on the equilibrium beach concept, the respective model structures and parameters associate different physical interpretations and shoreline behaviors (Section 2.4.1). Therefore, the uncertainty associated with the choice of the equilibrium modeling approach cannot be measured by direct confrontation of the S_s obtained with the two models, but requires consideration of the different model responses to the forcing conditions.

The results obtained for the two disequilibrium approaches (Y09 and SF) show similar seasonal and interannual shoreline cycles, although with notably different amplitudes. Such behaviors are rooted in the different expressions of the equilibrium physics adopted in the two wave-driven models (i.e., the mechanism that would drive the shoreline to an equilibrium position under constant wave conditions). Vitousek et al. (2021) analytically show that the type of equilibrium condition is critical for the short- and long-term

response of the shoreline model. On one hand, Y09's equilibrium condition depends on the current shoreline position, and is not influenced by storm events that occurred prior to a given time scale that is, implicitly defined by the model calibration (see "Appendix A" of Vitousek et al., 2021). On the other hand, SF's equilibrium state is determined by the (time varying) past wave conditions with an explicit "beach memory" function, and evolves in time accordingly. This means that, in absence of other processes, the Y09 modeled shoreline oscillates persistently around the same position regardless of the temporal variability of wave energy. Instead, SF can only achieve such a stable mean shoreline trend when forced with a periodic long-term wave climate (Vitousek et al., 2021). Hence, in presence of long-term trends of wave energy, Y09 emphasizes the short-term shoreline erosion/accretion in order to re-establish the equilibrium shoreline position, while SF adapts to the wave climate pattern. The latter results in larger amplitudes of seasonal fluctuations and in attenuation of long-term fluctuations, compared to SF.

The combined Y09 and Bruun models simulated shoreline ranges at 2100 are overall comparable to the ranges of the standalone Bruun Rule, indicating that in this scenario the net erosion modeled by 2100 is essentially driven by SLR. In fact, Y09 constrains the shoreline response to long-term wave climate shifts to a limited range (as described above) while the linearly added contribution of the Bruun model determines the shoreline trend. Instead, SF can produce wave-driven long-term shoreline trends that are combined with the Bruun retreat. This effect is observed in both RCP 4.5 and 8.5 scenarios, where the decreasing wave energy trend (Figures 2d and 2e) is translated by SF into shoreline accretion trends, resulting in less erosion than the Bruun model alone (Table 3).

Such properties of the two model behaviors highlight the different model sensitivities to long-term variability of the wave climate, which can have implications on the uncertainties in shoreline projections. Including the uncertainty of long-term wave climate variability in the ensemble projections would allow investigating the uncertainties related to the different behaviors of the shoreline models.

5.3. Model Free Parameters

Resolving process-based shoreline response to time-varying incident wave energy revealed that uncertainties in model parameters have the largest impact over the first simulated 30 years, regardless of the cross-shore shoreline model choice. Over this period, Y09 and SF uncertainties in response rate parameters ($k_y^{+/-}$ and k_s^+ , respectively) are responsible for most of the results uncertainties, which increases during low energy winters (on seasonal scale), and is particularly emphasized for SF in correspondence of extended low energy periods. This suggests that the assumption of a linear relationship between SF's response rate parameters ($k_s^- = r k_s^+$) may not hold in the context of long-term simulations, as it might depend on the evolution of waves properties (Ibaceta et al., 2020). In fact, Ibaceta et al. (2020) found that, such relation is not necessarily linear, indicating that the value of r may vary dynamically with changes in wave regimes. While the S_i s of the remaining model parameters (Φ for SF; a_1 and a_2 for Y09) show a definite seasonality, their variability on longer time scales is unclear. However, Φ 's S_i s, which exhibit relatively high values (up to 90%) at the beginning of the simulation, shows an overall decaying trend for both RCP scenarios applications. The a_1 and a_2 's S_i s remain weak, though not negligible, (<20%) over all the simulated period.

The behavior of the model free parameters' S_i s highlights, once again, the importance of wave energy variability in determining the impact of the parameters uncertainties on shoreline projections. This was also observed in previous studies, which showed that changes in wave regime can alter the model parameters and the functional relations between them (Ibaceta et al., 2020; Splinter et al., 2017). As a perspective of future work, one way to reduce the effects of model free parameters' uncertainties on modeled shoreline may be to employ non-stationary parameters that can adjust to changes in wave-climate regimes (Ibaceta et al., 2020). The use of non-stationary parameters would also imply a dynamic value of the r parameter, reducing uncertainties associated to the assumption of a linear relationship, between SF's response rate parameters. In addition, rearranging the Y09 parameters so that the new parameters have a similar order of magnitudes may increase the efficiency of model calibration, reducing model parameters uncertainties (Vitousek et al., 2021).

5.4. The Role of Wave Time Series

Our results indicate that the shoreline erosion is not only associated with large winter energy, but also depends on the trends of past winter wave energy and the internal variability of high-energy events within the season. For instance, in the RCP 4.5 scenario the winters 2084–2085 and 2059–2060 show similar 3-months averaged $H_s^2 T_p$ peak (164 and 172 m^2s , respectively), but they are preceded by several years of negative and positive winter energy trend, respectively (Figure 2b). This results in the winter 2084–2085 producing a rapid landward shift of shoreline position distribution, and the winter 2059–2060 driving more moderate annual changes while contributing to a long-term erosive trend (Figures 5c and 5d). We also observe that the interannual patterns of shoreline evolution are clearly correlated to those of winter wave energy. These behaviors underline the critical role of high/low energy winters interannual cycles, as well as storms sequencing, in wave-driven shoreline response, in line with previous studies (Besio et al., 2017; Dissanayake et al., 2015; Dodet et al., 2019). In addition, the temporal variability of wave climate (e.g., seasonal distribution of storm events) has been observed to affect the frequency (or “mode”) of shoreline response (Ibaceta et al., 2020; Splinter et al., 2017).

Therefore, we further investigated the potential role of future waves uncertainties in shoreline projections performing the GSA on an additional ensemble of 3,000 simulations forcing the Y09 and SF models with 100 different wave time series. We generated 100 random synthetic wave series using the method proposed by Davidson et al. (2017), which consists in building continuous series of wave conditions by sampling 1-month portions from a reference data set of existing wave data (e.g., historic wave data) at a given location. The method generates synthetic wave time series with random, though realistic, chronology of wave events, while maintaining the seasonal and yearly character of the wave climate. However, this assumes a long-term stationarity of the generated wave time series. We used the BW18 projections for the RCP 8.5 scenario as reference wave data. We individually applied the Davidson et al. (2017) method over 8 windows of 10 years from 2020 to 2100 in order to preserve the long-term (>10 years) characteristics of the reference time series while providing enough sampling reference data (Figure 9a). For instance, all the synthetic events from 2030 to 2040 were generated using monthly samples from the 2030–2040 reference data set.

When using the latter approach to generate ensemble waves the SF model shows some limitations. Therefore, here we exploit only the test results obtained with Y09. The results of the SF test application and the aforementioned limitations are illustrated in Text S5 and Figure S4 of Supporting Information.

The GSA shows that introducing uncertainties in the temporal distribution of wave events (Figure 9a) has a large impact on the variance of model results (Figure 9b) and, in turn, on the relative contributions of the remaining uncertain input parameters (Figures 9c–9h). In fact, accounting for uncertainty in wave events chronology (though in a simplistic way) increases the overall model variance throughout the entire simulated period (Figures 6c and 9b), and associates a dominating S_i (up to 0.3) over the first half of the simulated period (Figure 9i). However, SLR's S_i still emerges after 2060 and dominate shoreline projections uncertainties over the last two simulated decades. We also observe that the inclusion of wave chronology uncertainty attenuates the interannual variability of all S_i s while preserving the seasonal and 10-years signals (Figures 9c–9h). This is a natural consequence of the method used to generate the wave series ensemble. In fact, the Davidson et al. (2017) method is designed to preserve the seasonal variability, while its application to fixed time windows of the reference time series constrains the ensemble members to maintain the 10-years variability. The black lines in Figures 9c–9i show the time evolution of S_i s obtained removing the seasonal signal from the model results with a 1-year running average. When the seasonal variability of the results is removed, the SLR's S_i compensates the fluctuations of the model parameter's S_i s, resulting in an increased trend.

The test application illustrated above suggests that including uncertainties in short-term wave chronology can significantly impact the uncertainties of shoreline projections and the relative contributions of the remaining uncertain input variables. Further, introducing uncertainties on long-term non-stationarity of wave conditions would overcome the SF limitations occurring in this specific application, and may unveil new implications of the different Y09 and SF equilibrium approaches in the context of probabilistic long-term shoreline projections.

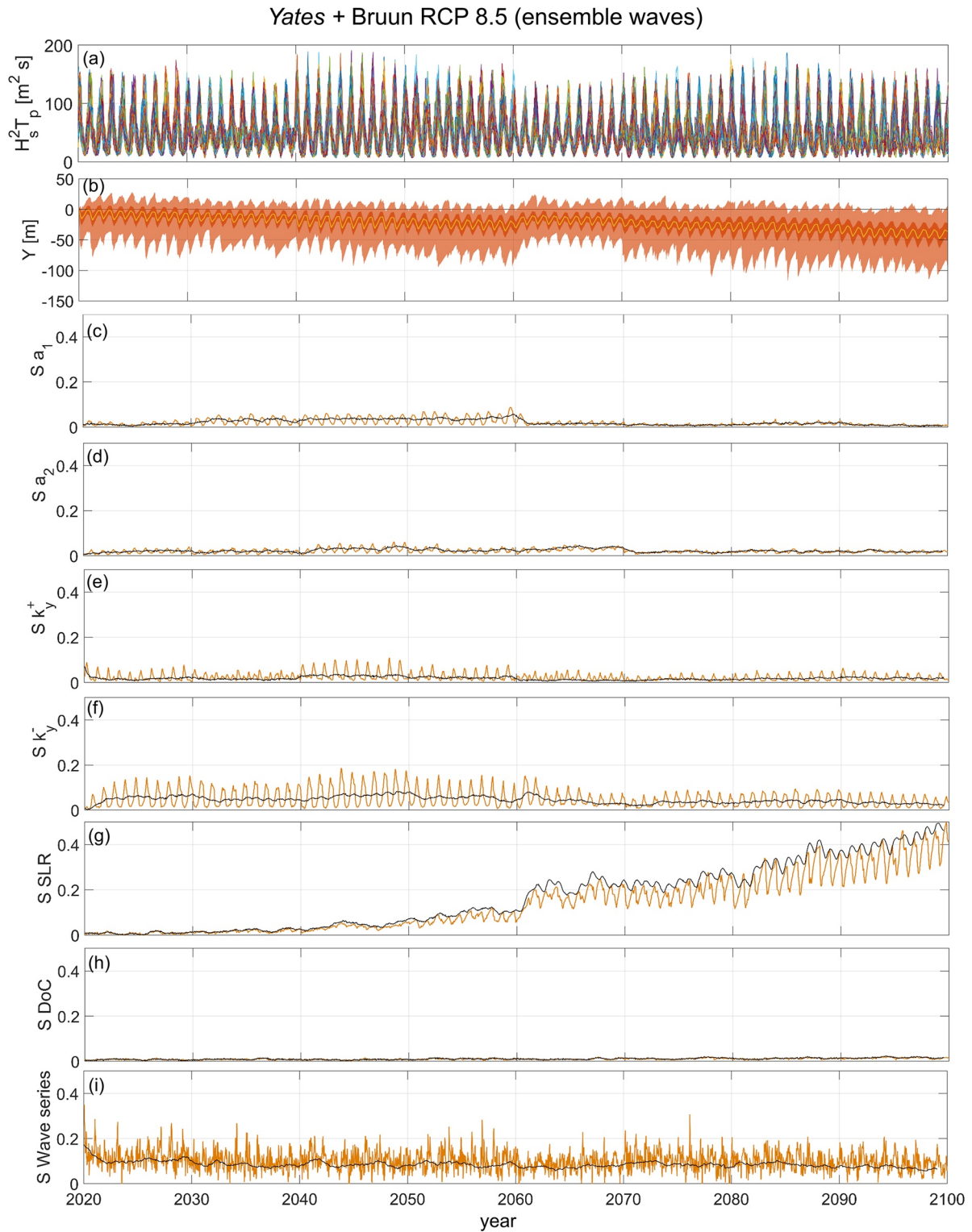


Figure 9. Ensemble of 3,000 *Yates* simulations forced using (a) 3-months average energy ($H_s^2 T_p$) of 100 random wave time series from 2020 to 2100 generated with the Davidson et al. (2017) method based on the BW18 wave projections for the RCP 8.5 scenario; (b) Ensemble shoreline projections over the analyzed period (dark/light shaded areas indicate the likely/envelope range, that is, variance (min-max), of shoreline position); First-order Sobol' index time series for (c) k_y^+ , (d) k_y^- , (e) a_1 , (f) a_2 , (g) sea-level rise, (h) depth of closure, and (i) wave energy, with respective time series calculated on the 1-year running average of model results (black lines).

5.5. Assumptions and Limitations

Wave projections are affected by uncertainties owing to the choice of the Global Climate Model (Morim et al., 2020) and random variability of wave events. Although our results are based on deterministic BW18's wave projections, in the northeast Atlantic region the estimated future wave statistics have been observed to be mostly sensitive to the RCP scenario (Morim et al., 2020). Yet, the use of deterministic wave projections hides a potentially large impact of the uncertain wave-climate variability on both shoreline predictions uncertainty and behavior of the shoreline models.

In addition, accounting for uncertainties in wave projections may also increase the uncertainties in DoC, which were based on one deterministic wave time series in the present study. However, to the authors' knowledge there is no other data set of continuous 2020–2100 wave projections, over the north Atlantic area, with a sufficient spatial resolution to resolve the site-specific regional scale processes. This underlines the need of continuous wave time series (obtained with different wave models of fine enough spatial resolution, different climate models, for different RCP scenarios), as well as tools allowing generating continuous realistic future wave time series, such as climate based stochastic wave emulators (D. Anderson et al., 2019; Cagigal et al., 2020).

In the current work, we assumed that MSL 2020–2100 projections are normally distributed. However, the MSL distribution may be skewed toward higher values due to additional uncertainty related to Antarctic ice-sheet melting in the RCP 8.5 scenario. We simulated a deterministic RCP 8.5 high-end SLR scenario to define a low-probability/high-impact scenario for projected shoreline erosion. Yet, our high-end SLR scenario is based on a particular combination of high-end contributions to sea-level rise, which makes no consensus in the scientific community (Bamber et al., 2019; Edwards et al., 2021; Stammer et al., 2019). While this is not included in the GSA, the use of a skewed probability distribution may lead to an earlier onset of SLR uncertainties in shoreline projections.

The Bruun Rule, used in our application to estimate SLR-driven shoreline recession, builds on several strong assumptions that reduce the applicability of this model to a limited range of beaches (Cooper et al., 2020). As the Truc Vert is an uninterrupted natural cross-shore transport dominated beach, with large sediment availability, most underlying assumption of the Bruun model are satisfied. However, alternative models to address beach response to SLR, such as *ShoreTrans* (McCarroll et al., 2020), can be implemented in this framework.

Coupling the Bruun Rule with Y09 and SF allows accounting for long-term effects of SLR while resolving short-term shoreline response to the wave climate. The Y09 and SF models do not explicitly resolve sediment exchange between the different beach compartments (e.g., upper beach and dune), and may fail reproducing episodic shoreline changes such as short-term accretion following to dune erosion events. However, if such events occur during the model calibration period, as in our applications (i.e., winter 2013–2014), their influence on the bulk shoreline response is partially accounted.

Here, we investigated the main effect of the uncertainties in input variables (S_i). While the estimated S_i of the DoC remains relatively low over the simulated period, in all simulated scenarios, the interaction of DoC and SLR uncertainties (i.e., *second-order Sobol' index*) may have a larger impact. However, estimating robust interaction terms would require a larger ensemble of simulations (several tens of thousands). Furthermore, in order to rigorously conclude on the negligible character of some uncertainties, GSA should be conducted within the factors' fixing setting (i.e., investigating the “total effect” of uncertain variables, Saltelli et al., 2008). In the presence of dependence among the inputs, more advanced GSA indices should be used for this purpose. In particular, a method that employs the so-called *Shapley effects* has recently been proposed and showed very promising results (Iooss & Prieur, 2019). While the direct application of this method requires computational cost of several order of magnitudes larger than the Sobol' indices (see Iooss & Prieur, 2019), Broto et al. (2020) successfully implemented a more computationally efficient sampling-based method for GSA using Shapley indices. This may be an interesting perceptible for future works.

6. Conclusions

We performed a Global Sensitivity Analysis on probabilistic 2020–2100 shoreline projections at the cross-shore transport dominated Truc Vert beach in southwest France. Time varying first-order Sobol' indices were calculated for sea-level rise, depth of closure, and model free parameters for two different cross-shore shoreline models (*Yates* and *ShoreFor*) and two RCP scenarios (RCP 4.5 and RCP 8.5). We show that uncertainties in shoreline projections are initially driven by uncertainties in model free parameters, with the effects of SLR uncertainties only emerging in the second half of the 21st century. However, the relative effects of SLR and model parameters uncertainties on shoreline projections do not only depend on the shoreline modeling approach and RCP scenarios, but their time evolution is also related to the forcing wave-climate variability. We also emphasize the importance of accounting for uncertainties related to the temporal distribution of wave energy, and therefore the need of ensembles of synthetic wave time series that account for the inherent variability of the wave climate.

Conflicts of Interest

The authors declare that there is no conflict of interest that could be perceived as prejudicing the impartiality of the research reported.

Data Availability Statement

All data used (wave, mean sea level and shoreline data) and produced (shoreline projections) in this work are available at <https://data.mendeley.com/datasets/gnvkx44t63/draft?a=a32c56ba-f495-4652-9eda-964dea31cec6>.

Acknowledgments

This work is co-financed by the BRGM and Make Our Planet Great Again (MOPGA) national program (Grant 927923G) and the BRGM (French Geological Survey). BC funded by Agence Nationale de la Recherche (ANR) grant number ANR-17-CE01-0014. GLC and RT are supported by H2020 ERA4CS ECLISEA (Grant 690462). This study includes the monitoring study site of Truc Vert labeled by the Service National d'Observation (SNO) Dynalit (<https://www.dynalit.fr>) with additional support from Observatoire Aquitaine de l'Univers (OASU) and Observatoire de la Côte Aquitaine (OCA). The authors thank the colleagues, including S. Bujan, S. Ferreira and V. Marieu involved in the topographic data; SONEL for past sea levels and vertical land motion data (<https://www.sonel.org/-GPS-.html>); and the Integrated Climate Data Center at the University of Hamburg (<https://icdc.cen.uni-hamburg.de/en/ar5-slr.html>) for SLR projections data. The authors are grateful to the reviewers (G. Coco, S. Vitousek and Anonymous reviewer), Associated Editor and Editor for their constructive remarks, which greatly improved this article.

References

- Allenbach, K., Garonna, I., Herold, C., Monioudi, I., Giuliani, G., Lehmann, A., & Velegarakis, A. F. (2015). Black Sea beaches vulnerability to sea level rise. *Environmental Science & Policy*, 46, 95–109. <https://doi.org/10.1016/j.envsci.2014.07.014>
- Anderson, D., Rueda, A., Cagigal, L., Antolínez, J. A. A., Mendez, F. J., & Ruggiero, P. (2019). Time-varying emulator for short and long-term analysis of coastal flood hazard potential. *Journal of Geophysical Research: Ocean*, 124(12), 9209–9234. <https://doi.org/10.1029/2019JC015312>
- Anderson, T. R., Fletcher, C. H., Barbee, M. M., Frazer, L. N., & Romine, B. M. (2015). Doubling of coastal erosion under rising sea level by mid-century in Hawaii. *Natural Hazards*, 78(1), 75–103. <https://doi.org/10.1007/s11069-015-1698-6>
- Angnuureng, A. B., Almar, R., Senechal, N., Castelle, B., Addo, K. A., Marieu, V., & Ranasinghe, R. (2017). Shoreline resilience to individual storms and storm clusters on a meso-macrotidal barred beach. *Geomorphology*, 290, 265–276. <https://doi.org/10.1016/j.geomorph.2017.04.007>
- Antolínez, J. A. A., Méndez, F. J., Anderson, D., Ruggiero, P., & Kaminsky, G. M. (2019). Predicting climate driven coastlines with a simple and efficient multi-scale model. *Journal of Geophysical Research: Earth Surface*, 124, 1596–1624. <https://doi.org/10.1029/2018JF004790>
- Athanasiou, P., van Dongeren, A., Giardino, A., Vousdoukas, M. I., Ranasinghe, R., & Kwadijk, J. (2020). Uncertainties in projections of sandy beach erosion due to sea level rise: An analysis at the European scale. *Scientific Reports*, 10, 11895. <https://doi.org/10.1038/s41598-020-68576-0>
- Bamber, J. L., Oppenheimer, M., Kopp, R. E., Aspinall, W. P., & Cooke, R. M. (2019). Ice sheet contributions to future sea-level rise from structured expert judgment. *Proceedings of the National Academy of Sciences*, 116(23), 11195–11200. <https://doi.org/10.1073/pnas.1817205116>
- Bertsimas, D., & Tsitsiklis, J. (1993). Simulated annealing. *Statistical Science*, 8(1), 10–15. <https://doi.org/10.1214/ss/1177011077>
- Besio, G., Briganti, R., Romano, A., Mentaschi, L., & De Girolamo, P. (2017). Time clustering of wave storms in the Mediterranean Sea. *Natural Hazards and Earth System Sciences*, 17, 505–514. <https://doi.org/10.5194/nhess-17-505-2017>
- Bricheno, L., & Wolf, J. (2018). Future wave conditions of Europe, in response to high-end climate change scenarios. *Journal of Geophysical Research: Oceans*, 123(12), 8762–8791. <https://doi.org/10.1029/2018JC013866>
- Broto, B., Bachoc, F., & Depecker, M. (2020). Variance reduction for estimation of Shapley effects and adaptation to unknown input distribution. *SIAM/ASA Journal on Uncertainty Quantification*, 8(2), 693–716. <https://doi.org/10.1137/18M1234631>
- Bruun, P. (1962). Sea-level rise as a cause of shore erosion. *Journal of the Waterways and Harbors Division*, 88(1), 117–130. <https://doi.org/10.1061/jwheau.0000252>
- Bruun, P. (1988). The Bruun rule of erosion by sealevel rise: A discussion on large-scale two- and three-dimensional usages. *Journal of Coastal Research*, 4(4), 627–648. Retrieved from www.jstor.org/stable/4297466
- Cagigal, L., Rueda, A., Anderson, D., Ruggiero, P., Marrifield, M. A., Montaña, J., et al. (2020). A multivariate, stochastic, climate-based wave emulator for shoreline change modelling. *Ocean Modelling*, 154, 101695. <https://doi.org/10.1016/j.ocemod.2020.101695>
- Casas-Prat, M., McInnes, K. L., Hemer, M. A., & Sierra, J. P. (2016). Future wave-driven coastal along the Catalan coast (NW Mediterranean). *Regional Environmental Change*, 16(6), 1739–1750. <https://doi.org/10.1007/s10113-015-0923-x>
- Castelle, B., Bujan, S., Marieu, V., & Ferreira, S. (2020). 16 years of topographic surveys of rip-channelled high-energy meso-macrotidal sandy beach. *Scientific Data*, 7, 410. <https://doi.org/10.1038/s41597-020-00750-5>
- Castelle, B., Dodet, G., Masselink, G., & Scott, T. (2017). A new climate index controlling winter wave activity along the Atlantic coast of Europe: The West Europe pressure anomaly. *Geophysical Research Letters*, 44(3), 1384–1392. <https://doi.org/10.1002/2016GL072379>

- Castelle, B., Dodet, G., Masselink, G., & Scott, T. (2018a). Increased winter-mean wave height, variability and periodicity in the North-East Atlantic over 1949–2017. *Geophysical Research Letters*, *45*(8), 3586–3596. <https://doi.org/10.1002/2017GL076884>
- Castelle, B., Guillot, B., Marieu, V., Chaumillon, E., Hanquez, V., Bujan, S., & Poppeschi, C. (2018b). Spatial and temporal patterns of shoreline change of a 280-km high-energy disrupted sandy coast from 1950 to 2014: SW France. *Estuarine, Coastal and Shelf Science*, *200*, 212–223. <https://doi.org/10.1016/j.ecss.2017.11.005>
- Castelle, B., Marieu, V., Bujan, S., Ferreira, S., Parisot, J., Capo, S., et al. (2014). Equilibrium shoreline modelling of high energy meso-macrotidal multiple barred beach. *Marine Geology*, *347*, 85–94. <https://doi.org/10.1016/j.margeo.2013.11.003>
- Castelle, B., Marieu, V., Bujan, S., Splinter, K. D., Robinet, A., Sénéchal, N., & Ferreira, S. (2015). Impact of the winter 2013–2014 series of severe Western Europe storms on a double-barred sandy coast: Beach and dune erosion and megacusp embayments. *Geomorphology*, *238*, 135–148. <https://doi.org/10.1016/j.geomorph.2015.03.006>
- Charles, E., Idier, D., Delecluse, P., Déqué, M., & Le Cozannet, G. (2012). Climate change impact on waves in the Bay of Biscay, France. *Ocean Dynamics*, *62*, 831–848. <https://doi.org/10.1007/s10236-012-0534-8>
- Church, J. A., Clark, P. U., Cazenave, A., Gregory, J. M., Jevrejeva, S., Levermann, A., et al. (2013). *Sea level change in climate change 2013: The physical science basis; contribution of working group I to the fifth assessment report of the intergovernmental panel on climate change*. Cambridge University Press.
- Coco, G., Senechal, N., Rejas, A., Bryan, K. R., Capo, S., Parisot, J. P., et al. (2014). Beach response to a sequence of extreme storms. *Geomorphology*, *204*, 493–501. <https://doi.org/10.1016/j.geomorph.2013.08.028>
- Cooper, J. A. G., Masselink, G., Coco, G., Short, A. D., Castelle, B., Rogers, K., et al. (2020). Sandy beaches can survive sea-level rise. *Nature Climate Change*, *10*, 993–995. <https://doi.org/10.1038/s41558-020-00934-2>
- Cooper, J. A. G., & Pilkey, O. H. (2004). Sea-level rise and shoreline retreat: Time to abandon the Bruun Rule. *Global and Planetary Change*, *43*(3–4), 157–171. <https://doi.org/10.1016/j.gloplacha.2004.07.001>
- D'Anna, M., Castelle, B., Idier, D., Le Cozannet, G., Rohmer, J., & Robinet, A. (2020). Impact of model free parameters and sea-level rise uncertainties on 20-years shoreline hindcast: The case of Truc Vert beach (SW France). *Earth Surface Processes and Landforms*, *45*(8), 1895–1907. <https://doi.org/10.1002/esp.4854>
- Davidson, M. A., Splinter, K. D., & Turner, I. L. (2013). A simple equilibrium model for predicting shoreline change. *Coastal Engineering*, *73*, 191–202. <https://doi.org/10.1016/j.coastaleng.2012.11.002>
- Davidson, M. A., Turner, I. L., Splinter, K. D., & Harley, M. D. (2017). Annual prediction of shoreline erosion and subsequent recovery. *Coastal Engineering*, *130*, 14–25. <https://doi.org/10.1016/j.coastaleng.2017.09.008>
- Dissanayake, P., Brown, J., Wisse, P., & Karunaratna, H. (2015). Comparison of storm cluster vs isolated event impacts on beach/dune morphodynamics. *Estuarine, Coastal and Shelf Science*, *164*, 301–312. <https://doi.org/10.1016/j.ecss.2015.07.040>
- Dodet, G., Castelle, B., Masselink, G., Scott, T., Davidson, M., Floch, F., et al. (2019). Beach recovery from extreme storm activity during the 2013–14 winter along the Atlantic coast of Europe. *Earth Surface Processes and Landforms*, *44*(1), 393–401. <https://doi.org/10.1002/esp.4500>
- Edwards, T. L., Nowicki, S., Marzeion, B., Hock, R., Goelzer, H., Seroussi, H., et al. (2021). Projected land ice contributions to 21st century sea level rise. *Nature*. (in Press)
- Frederikse, T., Landerer, F., Caron, L., Adhikari, S., Parkes, D., Humphrey, V. W., et al. (2020). The causes of sea-level rise since 1900. *Nature*, *584*(7821), 393–397. <https://doi.org/10.1038/s41586-020-2591-3>
- Ghermandi, A., & Nunes, P. A. L. D. (2013). A global map of coastal recreation values: Results from a spatially explicit meta-analysis. *Ecological Economics*, *86*, 1–15. <https://doi.org/10.1016/j.ecolecon.2012.11.006>
- Grinsted, A., Jevrejeva, S., Riva, R. E. M., & Dahl-Jensen, D. (2015). Sea level rise projections for northern Europe under RCP 8.5. *Climate Research*, *64*, 15–23. <https://doi.org/10.3354/cr01309>
- Hallermeier, R. J. (1978). Uses for a calculated limit depth to beach erosion. In: *Proceedings of the 16th Coastal Engineering Conference* (pp. 1493–1512). New York: ASCE. <https://doi.org/10.1061/9780872621909.090>
- Hazeleger, W., Wang, X., Severijns, C., Ștefănescu, S., Bintanja, R., Steri, A., et al. (2012). EC-Earth v2. 2: Description and validation of a new seamless Earth system prediction model. *Climate Dynamics*, *39*(11), 2611–2629. <https://doi.org/10.1007/s00382-011-1228-5>
- Hinkel, J., Church, J. A., Gregory, J. M., Lambert, E., Le Cozannet, G., Lowe, J., et al. (2019). Meeting user needs for sea level rise information: A decision analysis perspective. *Earth's Future*, *7*, 320–337. <https://doi.org/10.1029/2018EF001071>
- Hunter, J. R., Church, J. A., White, N. J., & Zhang, X. (2013). Towards a global regionally varying allowance for sea-level rise. *Ocean Engineering*, *71*, 17–27. <https://doi.org/10.1016/j.oceaneng.2012.12.041>
- Ibaceta, R., Splinter, K. D., Harley, M. D., & Turner, I. L. (2020). Enhanced coastal shoreline modeling using an ensemble Kalman filter to include nonstationarity in future wave climates. *Geophysical Research Letters*, *47*(22). <https://doi.org/10.1029/2020GL090724>
- Iooss, B., & Prieur, C. (2019). Shapley effects for sensitivity analysis with correlated inputs: Comparisons with Sobol' indices, numerical estimation and applications. *International Journal for Uncertainty Quantification*, *9*(5), 493–514. <https://doi.org/10.1615/Int.J.UncertaintyQuantification.2019028372>
- Jackson, L. P., & Jevrejeva, S. (2016). A probabilistic approach to 21st century regional sea-level projections using RCP and High-end scenarios. *Global and Planetary Change*, *146*, 179–189. <https://doi.org/10.1016/j.gloplacha.2016.10.006>
- Jevrejeva, S., Frederikse, T., Kopp, R. E., Le Cozannet, G., Jackson, L. P., & van de Wal, R. S. W. (2019). Probabilistic sea level projections at the coast by 2100. *Surveys in Geophysics*, *40*, 1–1696. <https://doi.org/10.1007/s10712-019-09550-y>
- Klingebiel, A., & Legigan, P. (1992). Carte Géologique et structure du Bassin de la Leyre. *Bulletin de l'Institut de Géologie du Bassin d'Aquitaine*, *1992*(51–52), p7–20.
- Kopp, R. E., Horton, R. M., Little, C. M., Mitrovica, J. X., Oppenheimer, M., Rasmussen, D. J., et al. (2014). Probabilistic 21st and 22nd century sea-level projections at a global network of tide-gauge sites. *Earth's Future*, *2*(8), 383–406. <https://doi.org/10.1002/2014EF000239>
- Kroon, A., de Schipper, M. A., van Gelder, P., & Arninkhof, S. G. J. (2020). Ranking uncertainty: Wave climate variability versus model uncertainty in probabilistic assessment of coastline change. *Coastal Engineering*, *158*, 103673. <https://doi.org/10.1016/j.coastaleng.2020.103673>
- Laporte-Fauret, Q., Marieu, V., Castelle, B., Michalet, R., Bujan, S., & Rosebery, D. (2019). Low-cost uav for high-resolution and large-scale coastal dune change monitoring using photogrammetry. *Journal of Marine Science and Engineering*, *7*(3), 63. <https://doi.org/10.3390/jmse7030063>
- Larson, M., Hogan, L. X., & Hanson, H. (2010). Direct formula to compute wave height and angle at incipient breaking. *Journal of Waterway, Port, Coastal, and Ocean Engineering*, *136*(2), 119–122. [https://doi.org/10.1061/\(ASCE\)WW.1943-5460.0000030](https://doi.org/10.1061/(ASCE)WW.1943-5460.0000030)
- Le Cozannet, G., Castelle, B., Bulteau, T., Ranasinghe, R., Wöppelmann, G., Rohmer, J., et al. (2019). Quantifying uncertainties of sandy shoreline change projections as sea level rises. *Scientific Reports*, *42*(9). <https://doi.org/10.1038/s41598-018-37017-4>

- Le Cozannet, G., Oliveros, C., Castelle, B., Garcin, M., Idier, D., Pedreros, R., & Rohmer, J. (2016). Uncertainties in sandy shorelines evolution under the Bruun rule assumption. *Frontiers of Marine Science*, 3, 49. <https://doi.org/10.3389/fmars.2016.00049>
- Lemos, C., Floc'h, F., Yates, M., Le Dantec, N., Marieu, V., Hamon, K., et al. (2018). Equilibrium modelling of the beach profile on a macrotidal embayed low tide terrace beach. *Ocean Dynamics*, 68(9), 1207–1220. <https://doi.org/10.1007/s10236-018-1185-1>
- Li, C., & Mahadevan, S. (2016). An efficient modularized sample-based method to estimate the first-order Sobol' index. *Reliability Engineering & System Safety*, 153, 110–121. <https://doi.org/10.1016/j.res.2016.04.012>
- Losada, I. J., Toimil, A., Muñoz, A., Garcia-Fletcher, A. P., & Diaz-Simal, P. (2019). A planning strategy for the adaptation of coastal areas to climate change: The Spanish case. *Ocean & Coastal Management*, 182, 104983. <https://doi.org/10.1016/j.ocecoaman.2019.104983>
- Luijendijk, A., Hagenaars, G., Ranasinghe, R., Baart, F., Donchyts, G., & Aarminkhof, S. (2018). The state of the World's beaches. *Scientific Reports*, 8, 6641. <https://doi.org/10.1038/s41598-018-24630-6>
- Masselink, G., Castelle, B., Scott, T., Dodet, G., Suanez, S., Jackson, D., & Floc'h, F. (2016). Extreme wave activity during 2013/2014 winter and morphological impacts along the Atlantic coast of Europe. *Geophysical Research Letters*, 43(5), 2135–2143. <https://doi.org/10.1002/2015GL067492>
- McCarroll, R. J., Masselink, G., Valiente, N. G., Scott, T., Wiggins, M., Kirby, J. A., & Davidson, M. (2020). A novel rules-based shoreline translation model for predicting future coastal change: ShoreTrans. (Under Review) <https://doi.org/10.31223/osf.io/y4kmv>
- Merken, J. L., Reimann, L., Hinkel, J., & Athanasios, T. V. (2016). Gridded population projections for the coastal zone under the Shared Socioeconomic Pathways. *Global and Planetary Change*, 145, 57–66. <https://doi.org/10.1016/j.gloplacha.2016.08.009>
- Michaud, H., Pasquet, A., Leckler, F., Baraille, R., Dalphiné, A., & Aouf, L. (2016). Improvements of the new French coastal wave forecasting system and application to a wave-current interaction study. In: *14th International Workshop on Wave Hindcasting and Forecasting & 5th Coastal Hazard Symposium SHOM & Meteo France*. <https://doi.org/10.13140/RG.2.2.13218.02243>
- Montaño, J., Coco, G., Antolínez, J. A. A., Beuzen, T., Bryan, K. R., Cagigal, L., et al. (2020). Blind testing of shoreline evolution models. *Scientific Reports*, 10(1), 2137. <https://doi.org/10.1038/s41598-020-59018-y>
- Morim, J., Hemer, M., Wang, X. L., Cartwright, N., Trenham, C., Semedo, A., et al. (2019). Robustness and uncertainties in global multivariate wind-wave climate projections. *Nature Climate Change*, 9, 711–718. <https://doi.org/10.1038/s41558-019-0542-5>
- Morim, J., Trenham, C., Hemer, M., Wang, X. L., Mori, N., Casas-Prat, M., et al. (2020). A global ensemble of ocean wave climate projections from CMIP5-driven models. *Scientific Data*, 7, 105. <https://doi.org/10.1038/s41597-020-0446-2>
- Nash, J. E., & Sutcliffe, J. V. (1970). River flow forecasting through conceptual models part I—a discussion of principles. *Journal of Hydrology*, 10, 282–290. [https://doi.org/10.1016/0022-1694\(70\)90255-6](https://doi.org/10.1016/0022-1694(70)90255-6)
- Neuman, B., Athanasios, T. V., Zimmermann, J., & Nicholls, R. J. (2015). Future coastal population growth and exposure to sea-level rise and coastal flooding—A global assessment. *Plos One*, 10(6), e0131375. <https://doi.org/10.1371/journal.pone.0131375>
- Nicholls, R. J. (1998). Assessing erosion of sandy beaches due to sea-level rise. *Geological Society, London, Engineering Geology Special Publications*, 15(1), 71–76. <https://doi.org/10.1144/GSL.ENG.1998.015.01.08>
- Oppenheimer, M. B. C., Glavovic, J., Hinkel, R., van de Wal, A. K., Magnan, A., et al. (2019). Sea level rise and implications for low-lying islands, coasts and communities. In H.-O. Portner, D. C. Roberts, V. Masson-Delmotte, P. Zhai, M. Tignor, E. Poloczanska, et al. (Eds.), *IPCC special report on the ocean and cryosphere in a changing climate*.
- Pariset, J. P., Capo, S., Castelle, B., Bujan, S., Moreau, J. M., Gervais, M., et al. (2009). Treatment of topographic and bathymetric data acquired at the Truc-Vert Beach (SW France) during the ECORS field experiment [Special issue]. *Journal of Coastal Research* 56. In: *Proceedings of the 10th International Coastal Symposium ICS*, (Vol. II, pp. 1786–1790). Retrieved from www.jstor.org/stable/25738097
- Perez, J., Menendez, M., Camus, P., Mendez, F. J., & Losada, I. J. (2015). Statistical multi-model climate projections of surface ocean waves in Europe. *Ocean Modelling*, 96, 161–170. <https://doi.org/10.1016/j.ocemod.2015.06.001>
- Poumadère, M., Bertoldo, R., Idier, D., Mallet, C., Oliveros, C., & Robin, M. (2015). Coastal vulnerabilities under the deliberation of stakeholders: The case of two French sandy beaches. *Ocean & Coastal Management*, 105, 166–176. <https://doi.org/10.1016/j.ocecoaman.2014.12.024>
- Ranasinghe, R. (2016). Assessing climate change impacts on open sandy coasts: A review. *Earth-Science Reviews*, 160, 320–332. <https://doi.org/10.1016/j.earscirev.2016.07.011>
- Ranasinghe, R. (2020). On the need for a new generation of coastal change models for the 21st century. *Scientific Reports*, 10, 2010. <https://doi.org/10.1038/s41598-020-58376-x>
- Ranasinghe, R., Callaghan, D., & Stive, M. J. F. (2012). Estimating coastal recession due to sea level rise: Beyond the Bruun rule. *Climatic Change*, 110, 561–574. <https://doi.org/10.1007/s10584-011-0107-8>
- Reguero, B. G., Losada, I. J., & Mendez, F. J. (2019). A recent increase in global wave power as a consequence of oceanic warming. *Nature Communications*, 10, 205. <https://doi.org/10.1038/s41467-018-08066-0>
- Robinet, A., Castelle, B., Idier, D., Le Cozannet, G., Déqué, M., & Charles, E. (2016). Statistical modeling of interannual shoreline change driven by North Atlantic climate variability spanning 2000–2014 in the Bay of Biscay. *Geo-Marine Letters*, 36(6), 479–490. <https://doi.org/10.1007/s00367-016-0460-8>
- Robinet, A., Idier, D., Castelle, B., & Marieu, V. (2018). A reduced-complexity shoreline change model combining longshore and cross-shore processes: The LX-Shore model. *Environmental Modelling & Software*, 109, 1–16. <https://doi.org/10.1016/j.envsoft.2018.08.010>
- Robin, N., Billy, J., Castelle, B., Hesp, P., Nicolae Lerma, A., Laporte-Fauret, Q., et al. (2021). 150 years of foredune initiation and evolution driven by human and natural processes. *Geomorphology*, 374, 107516. <https://doi.org/10.1016/j.geomorph.2020.107516>
- Rohmer, J., & Le Cozannet, G. (2019). Dominance of the mean sea level in high-percentile sea levels time evolution with respect to large-scale climate variability: A Bayesian statistical approach. *Environmental Research Letters*, 14(1), 014008. <https://doi.org/10.1088/1748-9326/aaf0cd>
- Saltelli, A., Ratto, M., Andres, T., Campolongo, F., Cariboni, J., Gatelli, D., et al. (2008). *Global sensitivity analysis: The premier The atrium, southern gate*. Chichester: Jhon Wiley & Sons Ltd.
- Santamaria-Gómez, A., Gravelle, M., Dangendorf, S., Marcos, M., Spada, G., & Wöppelmann, G. (2017). Uncertainty of the 20th century sea-level rise due to vertical land motion errors. *Earth and Planetary Science Letters*, 473, 24–32. <https://doi.org/10.1016/j.epsl.2017.05.038>
- Slangen, A. B. A., Carson, M., Katsman, C. A., van de Wal, R. S. W., Kohl, A., Vermeersen, L. L. A., & Stammer, D. (2014). Projecting twenty-first century regional sea-level changes. *Climatic Change*, 124, 317–332. <https://doi.org/10.1007/s10584-014-1080-9>
- Sobol', I. M. (2001). Global sensitivity indices for nonlinear mathematical models and their Monte Carlo estimates. *Mathematics and Computers in Simulation*, 55(1–3), 271–280. [https://doi.org/10.1016/S0378-4754\(00\)00270-6](https://doi.org/10.1016/S0378-4754(00)00270-6)
- Splinter, K., Carley, J. T., Golshani, A., & Tomlinson, R. (2014b). A relationship to describe the cumulative impact of storm clusters on beach erosion. *Coastal Engineering*, 83, 49–55. <https://doi.org/10.1016/j.coastaleng.2013>

- Splinter, K., Turner, I. L., & Davidson, M. A. (2013). How much data is enough? The importance of morphological sampling interval and duration for calibration of empirical shoreline models. *Coastal Engineering*, 77, 14–27. <https://doi.org/10.1016/j.coastaleng.2013.02.009>
- Splinter, K., Turner, I. L., Davidson, M. A., Bernard, P., Castelle, B., & Oltman-Shay, J. (2014a). A generalized equilibrium model for predicting daily to interannual shoreline response. *Journal of Geophysical Research: Earth Surface*, 119(9), 1936–1958. <https://doi.org/10.1002/2014JF003106>
- Splinter, K., Turner, I. L., Reinhardt, M., & Ruessink, G. (2017). Rapid adjustment of shoreline behavior to changing seasonality of storms: Observations and modelling at an open-coast beach. *Earth Surface Processes and Landforms*, 42(8), 1186–1194. <https://doi.org/10.1002/esp.4088>
- Stammer, D., Van de Wal, R. S. W., Nicholls, R. J., Church, J. A., Le Cozannet, G., Lowe, J. A., et al. (2019). Framework for high-end estimates of sea level rise for stakeholder applications. *Earth's Future*, 7(8), 923–938. <https://doi.org/10.1029/2019EF001163>
- Thiéblemont, R., Le Cozannet, G., Rohmer, J., Toimil, A., Alvarez-Cuesta, M., & Losada, I. (2021). Deep uncertainties in shoreline change projections: An extra-probabilistic approach applied to sandy beaches. *Natural Hazards and Earth System Sciences Discuss.* in review [preprint] <https://doi.org/10.5194/nhess-2020-412/>
- Thiéblemont, R., Le Cozannet, G., Toimil, A., Meyssignac, B., & Losada, I. J. (2019). Likely and high-end impacts of regional sea-level rise on the shoreline change of European sandy coasts under a high greenhouse gas emissions Scenario. *Water*, 11, 2607. <https://doi.org/10.3390/w1122607>
- Toimil, A., Camus, P., Losada, I. J., Le Cozannet, G., Nicholls, R., Idier, D., & Maspataud, A. (2020). Climate change driven coastal erosion modelling in temperate sandy beaches methods and uncertainty treatment. *Earth-Science Reviews*, 202, 103110. <https://doi.org/10.1016/j.earscirev.2020.103110>
- Toimil, A., Diaz-Simal, P., Losada, I. J., & Camus, P. (2018). Estimating the risk of loss of beach recreation value under climate change. *Tourism Management*, 68, 387–400. <https://doi.org/10.1016/j.tourman.2018.03.024>
- Toimil, A., Losada, I. J., Camus, P., & Diaz-Simal, P. (2017). Managing coastal erosion under climate change at regional scale. *Coastal Engineering*, 128, 106–122. <https://doi.org/10.1016/j.coastaleng.2017.08.004>
- Tolman, H. (2009). *User manual and system documentation of WAVEWATCH III-version 3.14 (Technical report)*. NOAA/NWS/NCEP/MMAB.
- Vitousek, S., Barnard, P. L., Limber, P., Erikson, L., & Cole, B. (2017). A model integrating longshore and cross-shore processes for predicting long-term shoreline response to climate change. *Journal of Geophysical Research: Earth surface*, 122(4), 782–806. <https://doi.org/10.1002/2016JF004065>
- Vitousek, S., Cagigal, L., Montaña, J., Rueda, A. C., Mendez, F. J., Coco, G., & Barnard, P. (2021). The application of ensemble wave forcing to quantify uncertainty of shoreline change predictions. *Journal of Geophysical Research: Earth Surface*, 126. (in Press) <https://doi.org/10.1029/2019JF005506>
- Vousdoukas, M. I., Ranasinghe, R., Mentaschi, L., Plomaritis, T. A., Athanasiou, P., Luijendijk, A., & Feyen, L. (2020). Sandy coastlines under threat of erosion. *Nature Climate Change*, 10, 260–263. <https://doi.org/10.1038/s41558-020-0697-0>
- Wainwright, D. J., Ranasinghe, R., Callaghan, D. P., Woodroffe, C. D., Jongejan, R., Dougherty, A. J., et al. (2015). Moving from deterministic toward probabilistic coastal hazard and risk assessment: Development of a modelling framework and application to Narrabeen Beach, New South Wales, Australia. *Coastal Engineering*, 96, 92–99. <https://doi.org/10.1016/j.coastaleng.2014.11.009>
- Wolinsky, M. A., & Murray, A. B. (2009). A unifying framework for shoreline migration: 2. Application to wave-dominated coasts. *Journal of Geophysical Research*, 114, F01009. <https://doi.org/10.1029/2007JF000856>
- Wong, P. P., Losada, I. J., Gattuso, J. P., Hinkel, J., Khattabi, A., McInnes, K. L., et al. (2014). Coastal systems and low-lying areas. In: *Climate change 2014: Impacts, adaptation, and vulnerability. Part A: Global and sectoral aspects. Contribution of working group II to the fifth assessment report of the intergovernmental panel on climate change* (pp. 361–409). Cambridge: Cambridge University Press.
- Wright, L. D., & Short, A. D. (1984). Morphodynamic variability of surf zones and beaches: A synthesis. *Marine Geology*, 56(1–4), 93–118. [https://doi.org/10.1016/0025-3227\(84\)90008-2](https://doi.org/10.1016/0025-3227(84)90008-2)
- Yates, M. L., Guza, R. T., & O'Reilly, W. C. (2009). Equilibrium shoreline response: Observations and modeling. *Journal of Geophysical Research*, 114(C9), C09014. <https://doi.org/10.1029/2009JC005359>

References From the Supporting Information

- Edwards, T. L., Brandon, M. A., Durand, G., Edwards, N. R., Gолledge, N. R., Holden, P. B., et al. (2019). Revisiting Antarctic ice loss due to marine ice-cliff instability. *Nature*, 566, 58–64. <https://doi.org/10.1038/s41586-019-0901-4>
- Taylor, K. E., Stouffer, R. J., & Meehl, G. A. (2012). An overview of CMIP5 and the experiment design. *Bulletin of the American Meteorological Society*, 93, 485–498. <https://doi.org/10.1175/BAMS-D-11-00094.1>